



We provide custom laboratory and pilot equipment to printed electronics research & industry

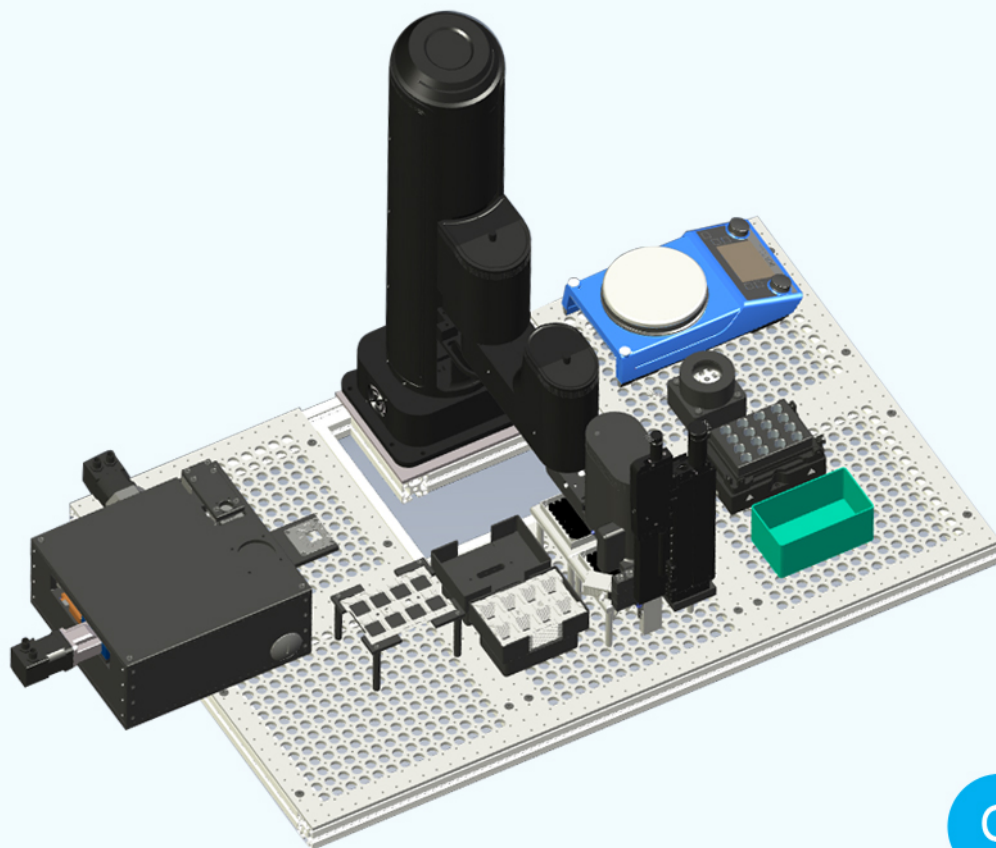
SpinBot One

a fully automated, customizable spin-coating robot

- **Graphical user interface** to control deposition process
- **Automated processing** of 100s of substrates
- 1 substrate per minute using **multiple spincoaters in parallel**
- Full **process control** and reproducibility
- **Database capability** storage of process parameters and measurement results per sample

Ready for

- **glovebox integration**
- integration of **characterization tools**
- **process integration to full devices** with electronic measurement tools and compatible to evaporation units



[Click to find out more](#)



Innovative automated scientific solutions

Application of Halide Perovskite Nanocrystals in Solar-Driven Photo(electro)Catalysis

Andrés F. Gualdrón-Reyes,* Camilo A. Mesa,* Sixto Giménez,* and Iván Mora-Seró*

Photo(electro)catalysis (PEC) is a promising strategy to conduct attractive solar-driven reactions such as CO₂ reduction to form added-value products, H₂ production, and organic substrates oxidation, taking advantage of the spatial separation of photocarriers generated in semiconductor-based electrodes. Halide perovskite nanocrystals (PNCs) are attracting increasing attention due to their tunable optical features and band structure, which is pivotal to modulate their oxidizing/reducing power and perform chemical reactions efficiently. However, the defective structure and ionic nature of PNCs make them prone to be unstable in polar media, where most of the relevant solar-driven chemical reactions of interest take place. In this review, an overview of recent strategies to stabilize PNCs in polar solvents is presented, some of them with promising application or already introduced in PEC systems. Perovskite encapsulation, including the formation of heterostructures, surface passivation engineering, and the synthesis of PNCs with intrinsic stability in polar media, is focused upon. Furthermore, perspectives for using stable lead-free PNCs in solar-driven PEC reactions are presented, showing the benefits of this future technology for energy production/transformation.

to store sunlight into chemical bonds. Commonly, PEC water splitting has been studied as an approach to reduce H⁺ to produce green hydrogen with the oxygen evolution reaction (OER) as electron donor. As this reaction is kinetically very demanding, water can be substituted by organic compounds as electron donors due to their faster oxidation kinetics. This would increase the H₂ evolution kinetics while concomitantly producing high added-value chemicals, remediating industrial wastewaters,^[3–8] and making use of semiconductor materials with highly oxidizing/reducing power.^[8,9] In a simple manner, when a semiconductor is illuminated with an energy equal or higher than its bandgap, charge carrier photogeneration and separation is promoted. Photogenerated holes are formed in the valence band (VB), where oxidation reactions take place, while electrons with higher free energy are located in the conduction band (CB) to trigger reduction reactions.^[9–11] This is

1. Introduction


Global warming and ecosystems contamination by fine chemicals industry have motivated to explore and develop cleaner and lower cost strategies for the energy conversion and transformation of organic compounds.^[1,2] Solar-driven catalysis via photo(electro)catalysis (PEC) has emerged as a promising route

the basis of photocatalytic (PC) reactions led through nanoparticle system (Figure 1A). Then, when the photomaterial is deposited in a conducting substrate, PEC oxidation and reduction reactions can be carried out in separate compartments.^[9,12,13] Here, one type of photocarriers migrate to the photoelectrode surface to conduct an interfacial PEC semireaction, while the other kind of photocarrier is transported through the external circuit to a counter electrode and perform the complementary PEC semireaction (Figure 1B).^[9]

Metal oxides, chalcogenides, and heterojunctions based on these materials have attracted significant attention as photocatalysts due to their wide gamut of low-cost synthetic protocols available for their preparation and facile charge carrier extraction.^[9,10,13–16] Although metal oxide photoelectrodes show a high performance under UV light, high stability, and low toxicity in some cases, they are often limited by their poor light harvesting efficiency toward near-infrared wavelengths. Additionally, metal oxide photoelectrodes tend to exhibit a fast carrier recombination as well as poor charge accumulation/transport kinetics, hindering their applicability in solar water splitting applications.^[10,17,18] In the case of chalcogenides, their superior optoelectronic properties are in contrast with the low stability promoted by their fast photodegradation. To reduce photodegradation and charge carrier recombination and to overcome charge transport/accumulation kinetic limitations, inner-sphere redox couples and organic substrates are commonly used to accelerate

A. F. Gualdrón-Reyes, C. A. Mesa, S. Giménez, I. Mora-Seró
Institute of Advanced Materials (INAM)
Universitat Jaume I
12071 Castelló de la Plana, Spain
E-mail: gualdron@uji.es; cmesa@uji.es; sjulia@fca.uji.es; sero@uji.es

A. F. Gualdrón-Reyes
Facultad de Ciencias
Instituto de Ciencias Químicas, Isla Teja
Universidad Austral de Chile
Valdivia 5090000, Chile

 The ORCID identification number(s) for the author(s) of this article can be found under <https://doi.org/10.1002/solr.202200012>.

© 2022 The Authors. Solar RRL published by Wiley-VCH GmbH. This is an open access article under the terms of the Creative Commons Attribution-NonCommercial-NoDerivs License, which permits use and distribution in any medium, provided the original work is properly cited, the use is non-commercial and no modifications or adaptations are made.

DOI: 10.1002/solr.202200012

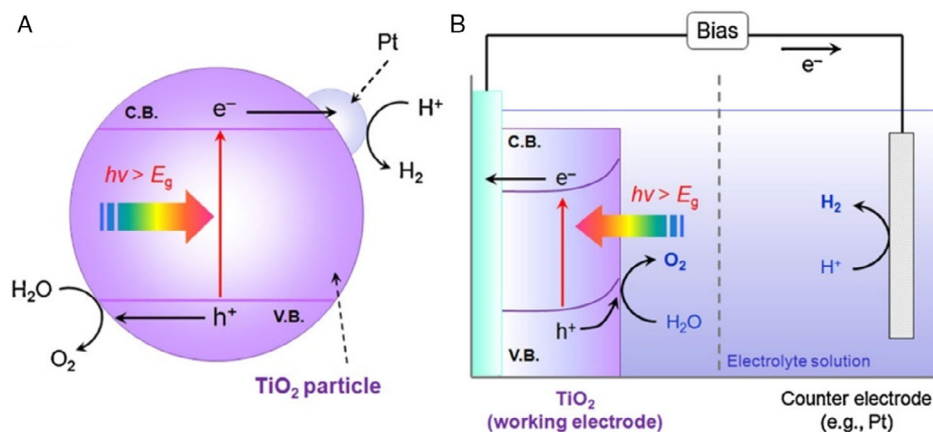


Figure 1. Schematic illustration of A) PC water splitting performed on nanoparticulated semiconductor and B) PEC water oxidation by using a semiconductor-based photoanode: holes are accumulated in the photocatalyst, while electrons are transported through the external circuit to a counter electrode. Reproduced with permission.^[9] Copyright 2011, Elsevier.

the electron transfer kinetics.^[19–25] Then, the preparation of photocatalysts with improved intrinsic properties is still a major challenge to develop novel materials with high potentiality in the field.

In this journey, halide perovskite nanocrystals (PNCs) are considered extremely competitive candidates.^[26,27] Owing to their outstanding features such as a tolerant-to-defect structure,^[28] photoluminescence quantum yield up to 100%,^[29,30] high carrier mobility,^[31] low cost, facile synthesis, and processing,^[32,33] PNCs have been successfully introduced in top-research applications such as solar cells,^[34] light-emitting diodes,^[35,36] photonics,^[37] photodetectors,^[38] and solar concentrators,^[39] among others. More interestingly, through particle size variation^[40] and composition engineering,^[41] bandgap and relative CB and VB positions can be modulated, providing to the PNCs an oxidizing or reducing power. Additionally, it has been reported that PNCs show a narrower bandgap than the classical photocatalysts,^[1,42] indicating a better capability to generate photocarriers for efficient PEC reactions. Our research group has been pioneering on studying the PEC properties of diverse PNCs based on CsBX_3 -type structure ($\text{B} = \text{Sn}^{2+}$, Pb^{2+} , $\text{X} = \text{Cl}^-$, Br^- , I^- , and combinations),^[43] establishing a relationship between both their nature and oxidizing or reducing capability. In this context, it is established that I-rich PNCs are more prone to inject electrons to a molecular acceptor species, while Cl, Br-rich PNCs are suitable to oxidize electron-rich species, accumulating more carriers into the photoactive material. Accordingly, a highly reducing CB minimum is exhibited to conduct CO_2 reduction,^[44] PC polymerization,^[45] and H_2 generation, while a VB maximum with high oxidizing power is reached for the degradation of organic molecules.^[41,46]

Nevertheless, the ionic interactions composing the PNCs crystal make them vulnerable to suffer structural modifications in polar solvents.^[47–49] This promotes that low-polar medium is ideal to preserve the perovskite integrity,^[50] but limiting the scope of PEC reactions where PNCs can be involved. Therefore, the state-of-the-art of PNC-based electrodes for conducting chemical reactions in polar media is limited, opening the door to the development of unprecedented long-term stable materials with improved PEC capability. As a first approach to

fabricate perovskite electrodes exposed to a polar environment, the use of perovskite bulk films stabilized in halide aqueous solutions to perform PEC hydrogen evolution reaction (HER) has been reported.^[51,52] Liu and co-workers^[52] fabricated TiO_2 nanorods (compact layer)/ MAPbI_3 perovskite-based heterostructures, using HI aqueous solution (57 wt%) saturated with MAPbI_3 powder as a supporting electrolyte. While MAPbI_3 crystals can oxidize a I^-/I_3^- redox couple,^[53] avoiding their degradation, electrons can be extracted to provide a HER rate around $33.3 \text{ mmol cm}^{-2} \text{ h}^{-1}$, with a Faradic efficiency close to 100% and a stable photocurrent density $\approx 2 \text{ mA cm}^{-2}$ for 8 h.

However, the eventual consumption of X^- to produce X_3^- promotes the decrease of X^- concentration into the aqueous solution, being harmful for mediating the perovskite stability.^[1] Accordingly, the addition of reducing agents such as H_3PO_2 is required to increase the content of X^- ,^[54] but these species are not compatible with the perovskite structure in some cases. Furthermore, the use of acid species to provide X^- anions (HX) makes that some cocatalysts are unstable in this environment, being difficult their selection. This fact clearly limits the maximum efficiency that this solar-driven reaction can provide. According to the above drawbacks, it is urgent to find novel strategies to achieve high-quality perovskite-based materials, with long-term stability in polar solvents to perform PEC reactions, extracting their maximum PEC capability.

In this review, we highlight innovative approaches to improve the stability of PNCs in polar environments, with high potential to fabricate photoelectrodes and perform the most challenging PEC reactions such as HER, oxygen evolution/reduction reactions (OER and ORR, respectively), CO_2 reduction, and remediation of industrial-waste organic compounds. Attractive alternatives such as material encapsulation and surface passivation processes are addressed to compensate structural defects and shield the PNCs from polar molecules. Furthermore, some synthetic protocols are introduced to produce PNCs with intrinsic ability to be directly exposed to polar environments, representing an ideal scenario for increasing the effectiveness of PEC performance. Lastly, we depict some contributions for using stable lead-free PNCs with prominent PEC activity, which would

allow the scaling up of PEC systems as eco-friendly future technologies to solve the demand of energy and environmental remediation issues.

2. PEC Properties of PNC-Based Photoelectrodes in Low-Polar Media

In this section, we will focus first in some approaches for PNC-based photoelectrodes in low-polar electrolytes reported in the current state of the art, to subsequently describe the current strategies to stabilize the PNCs in polar media.

As mentioned above, the structural nature of perovskites is the Achilles' heel to expand their applicability in polar environments mainly due to the liability of ionic species from the PbX_6 octahedra.^[55] In this context, the formation of a highly defective perovskite lattice would promote that external species such as H_2O and O_2 molecules interact with the photocatalyst matrix, breaking the crystalline structure^[56,57] and causing the progressive loss of the PL properties.^[58] The emergence of these defects (mainly halide deficiency) triggers the octahedra distortion and induces the phase transformation, from photoactive α -phase to nonactive δ -phase perovskites.^[59,60] Under this premise, perovskites in the form of bulk crystals are not suitable candidates to perform direct solar-driven chemistry in polar solvents, arising the need for the preparation of more tolerant-to-defect photomaterials with improved PL features under H_2O and oxygen

conditions. The synthesis of PNCs introduced by Pérez-Prieto and co-workers^[61] and then by Kovalenko and co-workers^[28] provided a suitable platform to obtain nanoconfined materials, where octahedra tilting is restrained, which can support the preparation of stable photocatalysts with the ability to resist low-polar oxygenated solvents, and conduct PEC oxidation/reduction reactions.

Green-emitting CsPbBr_3 nanoparticles have been used for CO_2 reduction in 0.1 M tetrabutylammonium hexafluorophosphate (TBAPF_6) in ethyl acetate (EtOAc) mixed with trace amounts of water as hole scavengers (volume ratio: 300:1). By using these nanoparticles combined with conductive transporters such as graphene oxide (GO), Kuang and co-workers^[62] have demonstrated that the composite material can generate a higher photocurrent $\approx 55 \mu\text{A cm}^{-2}$ (at -0.4 V versus Ag/AgCl) than pristine PNCs, indicative of the improved carrier separation and electron accumulation for reduction reactions (Figure 2A). In this way, CO_2 was transformed in added-value products such as CO and CH_4 and H_2 after 12 h of reaction. While low traces of H_2 were generated ($\approx 1.58 \mu\text{mol g}^{-1}$), higher fractions of CO and CH_4 (≈ 58.7 and $29.6 \mu\text{mol g}^{-1}$, respectively) were produced (Figure 2B). Other kinds of photoelectrodes based on GO-wrapped MAPbBr_3 PNCs have also been introduced in this PEC system. Here, Shen and co-workers^[63] demonstrated that GO can protect the nanocrystals from organic solvents, as the case of propylene carbonate, providing an efficient CO_2 reduction

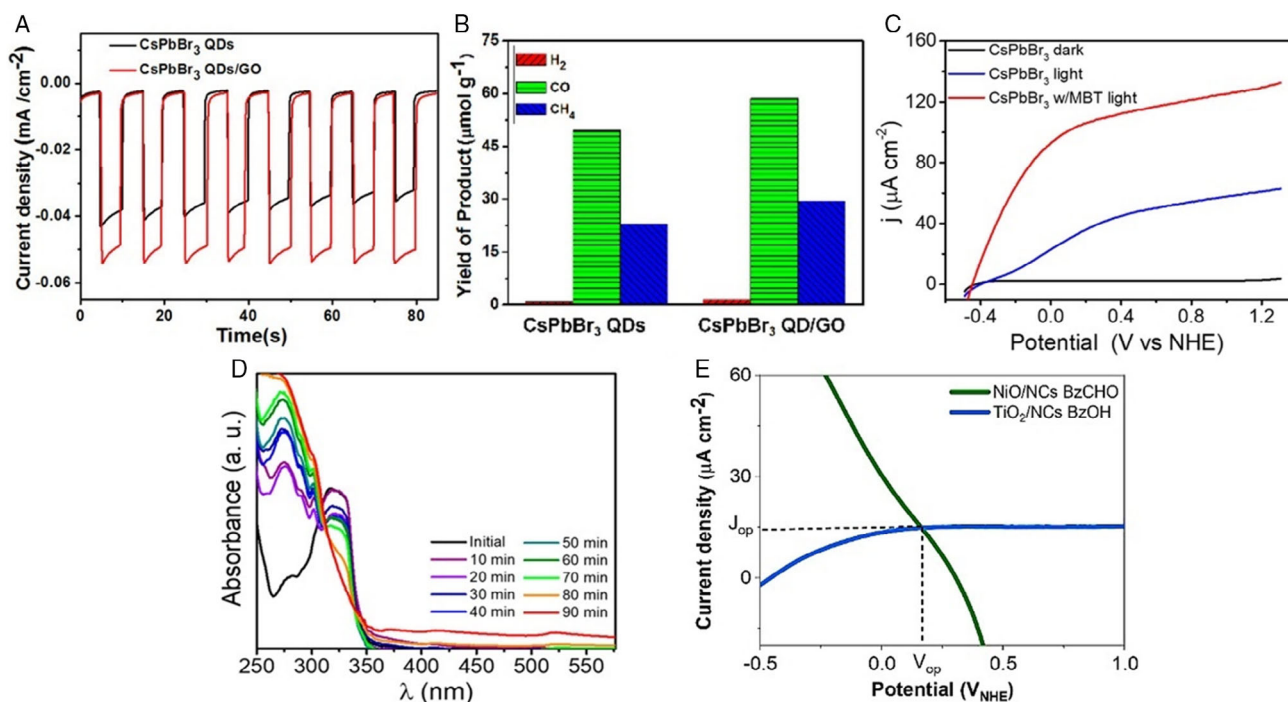


Figure 2. A) Photocurrent transient measurements (at -0.4 V versus Ag/AgCl) and B) photocatalytic (PC) CO_2 reduction to add-value products by using $\text{CsPbBr}_3/\text{GO}$ photocatalysts in 0.1 M TBAPF_6 ethyl acetate/ H_2O medium (AM1.5G illumination). Reproduced with permission.^[62] Copyright 2017, American Chemical Society. C) Linear sweep voltammetry measurements for CsPbBr_3 PNCs electrodes in the presence and absence of 2-MBT in 0.1 M $\text{TBAPF}_6/\text{dichloromethane}$. D) Absorbance spectra for PC 2-MBT oxidation in the presence of CsPbBr_3 PNCs (visible illumination). Reproduced under the terms of the CC-BY license.^[43] Copyright 2019, The Authors. Published by American Chemical Society. E) Operation of a tandem photoanode/photocathode fuel cell for a photo-assisted BzOH/BzCHO oxidation/reduction reaction in dichloromethane. Reproduced with permission.^[66] Copyright 2021, John Wiley & Sons, Inc

to CO and CH₄ with performances ≈ 0.525 and $0.025 \mu\text{mol g}^{-1}$, respectively. In line with how carbonaceous materials support an efficient carrier separation into a PNCs-based photoanode, Kuang and co-workers^[64] showed the PEC activity of mixed halide CsPbBr_{3-x}I_x PNCs/carbon nanotubes (CNT) photoelectrodes, in 0.1 M TBAPF₆, in dichloromethane, with 4 mM benzoquinone electron scavenger (organic reduction). By establishing an I/Br ratio = 1:1 ($x = 1.5$), the photocurrent is largely boosted to generate $420 \mu\text{A cm}^{-2}$, which is 7.7-fold higher than CsPbBr₃/CNT prototype. CNT accelerate the photogenerated electron-hole separation, which reduces the carrier recombination in the photoelectrode. Higher concentrations of CNT hinder the light absorption, which decreases the PEC capability of the photomaterial. In this sense, a compromise between CNT content and halide ratio is pivotal to produce a high photoresponse.

From the works discussed above, the use of nonpolar solvents is pivotal to preserve the structural integrity of PNCs and obtain valuable information about their activity in PEC reactions. However, this performance can also be influenced by alternative reactions taking place in the nonpolar system. Although authors have selected EtOAc as an adequate environment to ensure the stability of PNCs and facilitate the CO₂ dissolution, they have also concluded that this solvent undergoes partial photooxidation in the presence of PNCs to produce CO and CO₂ (average rate ≈ 0.56 and $2.52 \mu\text{mol g}^{-1} \text{h}^{-1}$, respectively).^[62] This observation was conducted replacing CO₂ by N₂ atmosphere for a control experiment. As traces of water into the nonpolar environment can react with some EtOAc molecules to form ethanol and acetic acid (ester hydrolysis), these C-species are prone to react in the PNCs/solution interface and produce the abovementioned CO and CO₂. In this context, it can be deduced that 1) part of the produced CO during photocatalytic CO₂ reduction comes from the EtOAc oxidation, and 2) more CO₂ molecules formed by this reaction will be available to react with PNCs and produce the expected added-value species. Therefore, the performance of the total process is increased. On the other hand, the formation of CO and CO₂ could also be promoted by the carbonaceous materials such as GO decomposition, which have been reported to occur by increasing the temperature from 50 °C.^[65] Although this work does not mention the value of this parameter, the continuous irradiation for 12 h can induce this increase, favoring the release of oxygenated groups from GO. Thus, control experiments with the use of ¹³C labeling are essential to clarify the effect of the solvent photo-oxidation/material decomposition on the net performance of solar-driven reaction.

Then, in PEC oxidation reactions, we have established the degradation of 2-mercaptobenzothiazole (2-MBT) (Figure 2C, D) and benzyl alcohol (BzOH) through CsPbBr₃ PNCs electrodes in 0.1 M TBAPF₆, in dichloromethane.^[43,66] In both systems, the photoanodes generate a higher photocurrent in the presence of the organic substrate. This fact describes the efficient oxidation of the target molecule on the PNCs/electrolyte interface, transferring electrons to the photoelectrode which are transported through the external circuit of the cell. Here, the total degradation of 2-MBT was achieved after 120 min of reaction. In the case of BzOH oxidation to benzaldehyde (BzCHO), a conversion yield around 12% was achieved. In addition, by fabricating different heterostructures between CsPbBr₃ PNCs/metal oxides (such as TiO₂, NiO), selective oxidation/reduction reactions can be

conducted, concluding that the PEC behavior of the photoelectrodes can be tailored. A proof-of-concept tandem system of photoanode/photocathode with the same photoactive inorganic halide perovskite, CsPbBr₃, was demonstrated for the photoelectrochemical BzOH/BzCHO oxidation/reduction (Figure 2E).^[66] Even PNCs are exhibited to be efficient to trigger the oxidation/reduction of organic compounds; next step is to identify the reaction intermediates or products, with the purpose to elucidate a mechanism of molecule conversion during the PEC process.

With the aim to extend the use of PNCs not only to low polar, but to high polar solvents and perform more complex multielectron reactions (such as the water splitting reaction to produce green hydrogen), PNCs stability is key. Thus, the following section reviews the current strategies to stabilize PNCs in polar media, from encapsulation and passivation to alternative synthetic routes.

3. Strategies to Stabilize PNCs in Polar Media

3.1. Encapsulation of PNCs—Formation of Heterostructures

The use of inorganic protective layers to promote the formation of a heterostructure through interfacial engineering stands out as a promising route to provide stability to halide perovskites.^[67–70] This strategy can be useful to avoid the direct contact of the nanocrystals with the polar molecules, without blocking the incident light to reach the photomaterial for the photogeneration of carriers. For example, Zhang and co-workers^[71] have developed the encapsulation of CsPbBr₃ PNCs with bulk Ni₂P to conduct efficient HER in a phosphate-buffered (PB) saline solution. This robust material is stable in the presence of water and O₂, avoiding the nanocrystals degradation. By reaching a CsPbBr₃: Ni₂P molar ratio = 1:6, CsPbBr₃@Ni₂P photocathodes provided a benchmark and reversible photocurrent up to $900 \mu\text{A cm}^{-2}$ during HER, after 5 light on/off cycles, higher than pristine CsPbBr₃ (Figure 3A), and stable during 12 h of reaction (first 1.5 h, the composite was under chopped light illumination, followed by 9 h of continuous irradiation, and finally, 1.5 h of chopped light). A Faradaic efficiency nearly 100% was reached (Figure 3B). Advantages such as bandgap narrowing and the faster HER kinetics from CsPbBr₃@Ni₂P make that the HER processes provide a 10 000-fold improvement compared to pristine PNCs. Then, after PEC reaction, transmission electron microscopy (TEM) and high-angle annular dark-field imaging scanning transmission electron microscopy (HAADF-STEM) revealed that the typical core/shell morphology achieved for the CsPbBr₃@Ni₂P was still preserved (inset of Figure 3B). In this line, long-term stability of CsPbBr₃@Ni₂P is associated to the protective coverage provided by Ni₂P, inhibiting the permeation of oxygen and water molecules, avoiding the PNCs aggregation, and guaranteeing a high conductivity to improve the carrier mobility through the composite material. Furthermore, authors have associated the close interaction between PNCs and Ni₂P to the formation of new Br–P bonds, which act as the carrier transfer channels, favoring the carrier accumulation in Ni₂P to enhance its high electrocatalytic activity to HER.

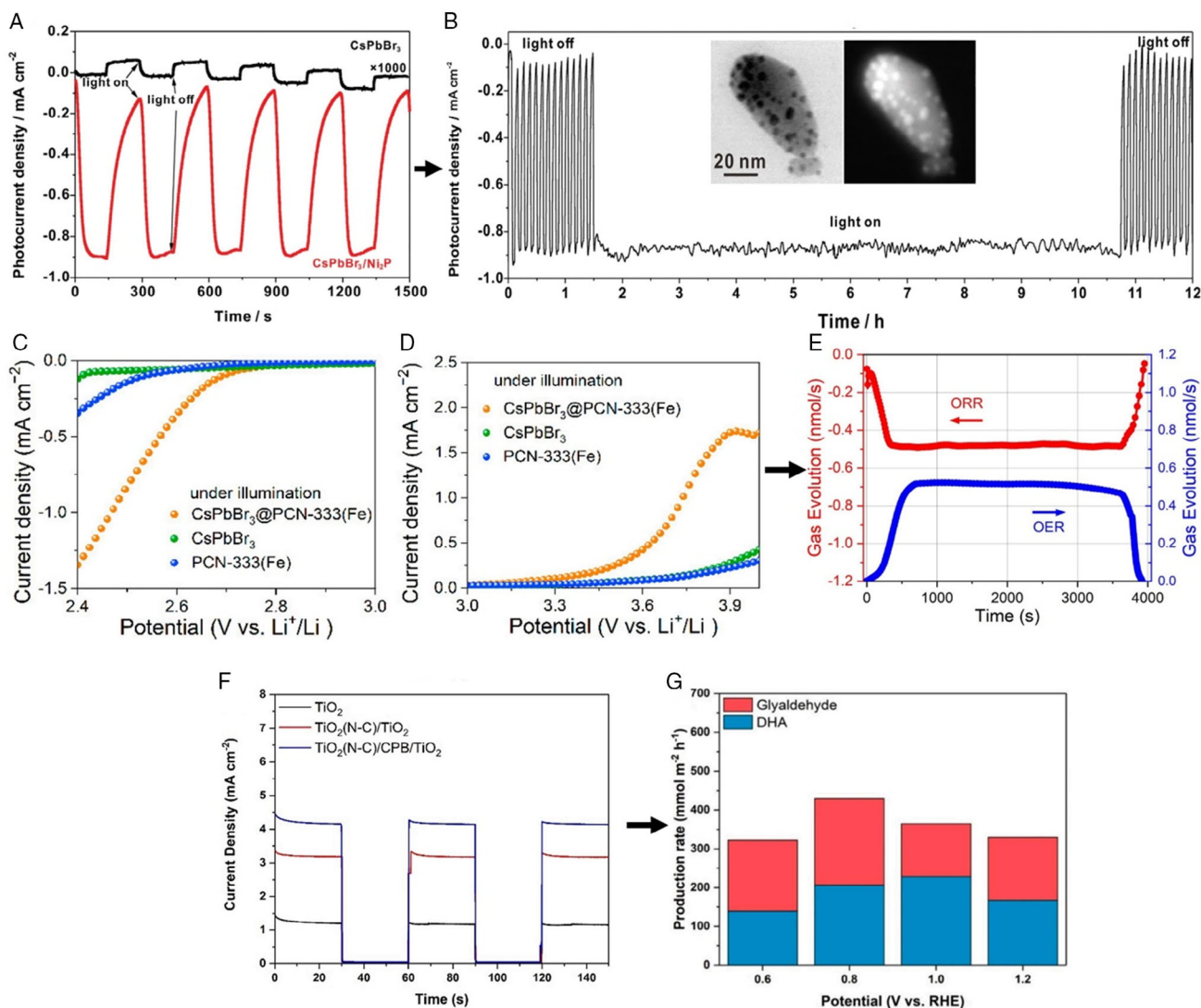


Figure 3. A) PEC behavior and B) stability measurements for CsPbBr₃ PNCs/Ni₂P heterostructures in 0.01 M PB at pH 7.4 (at 0 V versus RHE, simulated solar light, AM1.5G). Inset of Figure 3B shows the typical TEM and HAADF-STEM images of the composite material after stability test. Reproduced with permission.^[71] Copyright 2021, John Wiley & Sons, Inc. PEC activity of CsPbBr₃@PCN-333(Fe), PCN-333(Fe), and CsPbBr₃ materials. C) ORR and D) OER in 1 M LiTFSI/TEGDME under illumination. E) Determination of gas consumption and evolution during the ORR and OER processes through in-situ DEMS measurements for CsPbBr₃@PCN-333(Fe). Reproduced with permission.^[80] Copyright 2021, American Chemical Society. F) Photocurrent transient measurements for TiO₂(N-C)/CPB/TiO₂ and reference photoanodes, and G) PEC production rate for TiO₂(N-C)/CPB/TiO₂ in 0.1 M Na₂SO₄/glycerol aqueous solution (at 1.2 V versus RHE, pH 2) for TiO₂(N-C)/CPB/TiO₂ photoanode. Reproduced with permission.^[81] Copyright 2021, Elsevier

One of the most successful encapsulation agents to preserve the intrinsic properties of PNCs from polar environment appears to be mesoporous silica (m-SiO₂),^[72–74] which is considered a highly thermal, chemically stable, nontoxic, and cheap protective layer. For example, Manna and co-workers^[75] introduced molten salts such as KNO₃, KBr, and NaNO₃ to prepare solvent-free CsPbBr₃ PNCs/m-SiO₂ composites under air conditions and mild temperatures (≈350 °C). Depending on the stoichiometry of the salts, the sealing of silica pores is favored, making that the final composite delivers a PLQY ≈89 ± 10%, keeping their PL features for 3 h at 180 °C, and long-term stability in both water and aqua regia conditions for 1 month (stability was observed by measuring the PLQY under UV excitation light). These materials

also maintain their luminescence in saline water (Mⁿ⁺Cl_n; M = Na⁺, Ca²⁺, Mg²⁺, Na₂SO₄, NaHCO₃) and T = 90 °C for 24 h. Accordingly, the composition of the molten salts mixture shows an effect on the structure, stability, and final optical properties of the CsPbBr₃/m-SiO₂ composites. While NaNO₃ can modulate the porosity of the m-SiO₂ structure, the addition of KNO₃ and KBr increases the PL features of the PNCs, mainly PLQY. Although the authors acknowledge that the reasons to improve the photophysical features of the nanocrystals are unclear, it is clear that the species such as K⁺ and Br⁻ are pivotal to passivate their intrinsic structural defects.^[76] This is the main explanation of the role of molten salts to improve the stability of CsPbBr₃/m-SiO₂ in those harsh conditions. In this way, the

fabrication of PNCs electrodes by using this approach would provide long-term stability of nanocrystals in saline aqueous conditions, favoring important reactions such as HER and be competitive with classical encapsulation procedures.

Even though SiO₂ is largely employed to stabilize PNCs and maintain them separated from polar species, in some cases their 1D channels do not match with the particle size or geometry of the nanocrystals. This fact produces limited interactions and the escaping of photomaterial from the oxide matrix. In this context, metal–organic frameworks (MOFs) have emerged as an interesting class of highly ordered material, which is built by metal ions/clusters, and organic structures linked by coordination bonds.^[77–79] Here, Yu and co-workers^[80] have encapsulated CsPbBr₃ PNCs with Fe-MOFs based on PCN-333(Fe) (CsPbBr₃@PNC-333(Fe)), which shows large cages for the accommodation of PNCs, high chemical stability. This composite was studied in ORR and OER, respectively, in a aprotic polar environment consisting of 1 M lithium bis(trifluoromethanesulphonyl)imide/tetraethylene glycol dimethyl ether (LiTFSI/TEGDME). Under illumination CsPbBr₃@PCN-333(Fe) shows the highest currents and the lowest onset potentials for conducting ORR (Figure 3C) and OER (Figure 3D) compared to their individual counterparts. As an adequate heterostructure is established between PNCs and Fe-MOF, electrons can be easily transferred from PNCs to PCN-333(Fe) via the CB to favor the PEC ORR, while photogenerated holes are transported in opposite direction via the VB, providing highly oxidizing power for OER. Thus, by carrying out differential electrochemical mass spectrometry (DEMS) (Figure 3E) the O₂ evolution/consumption during the complete process was 1.77 μmol of O₂ in the ORR and 1.74 μmol of O₂ for reversed OER, stable for more than 1 h. Similar to Ni₂P encapsulation from the previous example, the authors propose the use of Fe-MOF as an impermeable layer to polar species, maintaining the structural integrity of the PNCs. Then, (although not suggested by the authors), a direct interaction between Br[−] anions from PNCs and Feⁿ⁺ (*n* = 2, 3) cations from the MOF can take place into the CsPbBr₃@PCN-333(Fe) material, which could explain the enhancement of the carrier separation and transport to the MOF. Although the Fe-MOF can isolate the PNCs from the ORR and OER processes, the eventual reduction in the catalytic property after 1 h can be attributed to the progressive migration of the polar environment through the MOF microporous cage, damaging the PNCs. At this stage, diverse formulations to prepare MOFs with balanced porous size and high catalytic activity will be ideal to be studied, and thereby prolong the lifetime of the PNCs.

Thus, in the line of preparation of MOFs to combine with PNCs, Huang and co-workers^[81] have fabricated hierarchical photoanodes based on MOFs derivatives N-doped carbon TiO₂/CsPbBr₃/TiO₂ nanorods (TiO₂(N-C)/CPB/TiO₂) to perform the PEC glycerol oxidation into added-value products. Here, the MOF derivative mediates a better carrier transfer capability from PNCs, increasing the interfacial carrier transfer into the composite. This composite is stable for a 0.5 h operation under UV–vis illumination in an 0.1 M Na₂SO₄ acid aqueous solution (pH 2), generating an optimized photocurrent ≈4.5 mA cm^{−2} (at 1.2 V versus RHE) during glycerol oxidation (Figure 3F). Establishing a chemical interaction between pyrrolic N from MOFs acting as electron donor (Lewis acid) and Br atoms

from PNCs acting as carrier acceptor (Lewis base), a new N–Br interaction emerges, stabilizing the structure of the PNCs, being this chemical bond the direct transfer channel to accumulate electrons in the TiO₂ nanorods and then transport them to the external circuit of the cell. Therefore, the carrier recombination into the composite is delayed, maximizing the light harvesting and favoring the accumulation of holes in the composite. In this context, the composite can transform glycerol to glyceraldehyde and 1,3-dihydroxyacetone, with a production rate near to 450 and 140 mmol m^{−2} h^{−1}, respectively (Figure 3G). In summary, it is concluded that the close interaction between PNCs and the protective layer through the appearance of new chemical bonds is the key factor to extend the long-term stability of the PNC-based photoelectrodes in polar environments and accelerate the carrier transfer into the composites.

3.2. Surface Passivation Engineering

Unlike encapsulation strategies, where the PNCs are entirely separated from the electrolyte, surface passivation strategies aim to compensate structural defects of perovskite based materials to decrease the nonradiative recombination channels.^[29,82] This is desirable to conduct the carrier separation and reaction with the surrounding environment more efficiently. A potential surface passivation strategy to apply in PNCs is reported by Kuang and co-workers^[83] who performed the photoelectrosynthesis of 2,5-dimethoxy-2,5-dihydrofuran (DMDF) in 0.36 M methylammonium bromide (MABr), acetonitrine/MeOH solution in the presence of Br[−]/Br⁺ redox couple, by using MAPbBr₃ single-crystal electrodes passivated with amorphous Al₂O₃ and Ti thin layers. These layers were deposited by atomic layer deposition (ALD). As a first step in the Al₂O₃ deposition, the formation of Br₃Pb–Al(CH₃)₃–PbBr₃ intermediates is promoted in the perovskite surface, which reacts with oxygen and give the above metal oxide. In this way, oxygen is found to passivate Pb-rich surface defects in the photomaterial, suppressing trap-assisted recombination. The defect compensation by oxygen has been described to restore the PL features in perovskites.^[84] Therefore, a photocurrent of 5.5 mA cm^{−2} was achieved during the PEC reaction by adjusting a suitable Al₂O₃ thickness of 5 nm (Figure 4A), indicating the modulation of oxygen content to interact with perovskite. Then, the Ti protective layer deposition mediates the formation of an ultrathin TiO_{2−x} film, increasing of the photocurrent up to 7.8 mA cm^{−2} and avoiding the contact of the single crystals with the polar media. At this point, TiO_{2−x} is a cocatalyst of Br oxidation, reducing the applied potential to conduct this PEC reaction (from 0.8 V through electrocatalysis, to 0.2 V in this contribution) (Figure 4B). Interestingly, the photocurrent is stable for 6 h, giving a Faradaic efficiency as high as 93% for the DMDF production. Although the authors do not emphasize the effect of the electrolyte in the long-term stability of the electrode, it appears that the presence of MABr is not only useful to promote the production of DMDF, but also to passivate halide vacancies similar to oxygen from Al₂O₃ layer discussed above. This fact would support the emergence of a less defective material and more resistant to polar solvents.

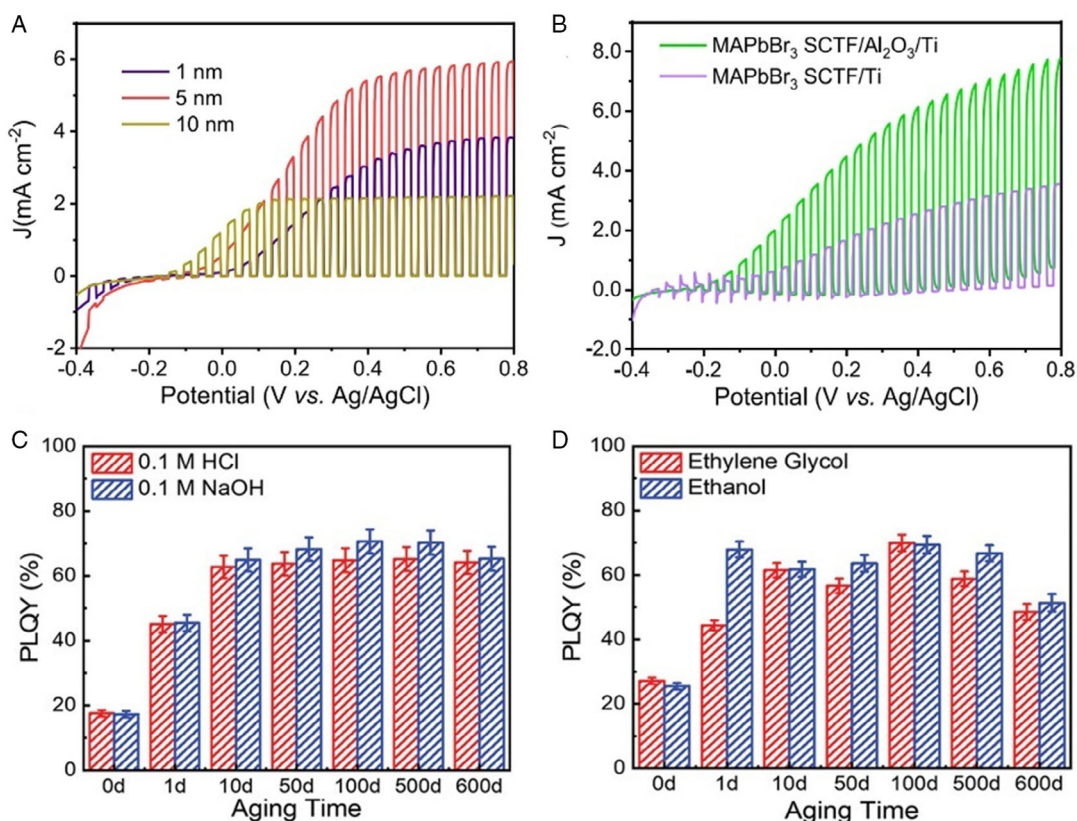


Figure 4. PEC behavior of MAPbBr₃ single crystals based electrodes A) passivated with Al₂O₃ layer deposited by ALD technique, by varying the thickness layer and B) after TiO_{2-x} thin layer as cocatalyst in 0.36 M MABr, acetonitrile/methanol solution. Reproduced under the terms of the CC-BY license.^[83] Copyright 2021, The Authors. Published by Springer Nature. PLQY stability measurements for methylmetacrylate-functionalized MAPbBr₃ PNCs in C) in acid and base solutions, and D) in ethylene glycol and ethanol media. Reproduced with permission.^[85] Copyright 2020, John Wiley & Sons, Inc.

Meanwhile, Lee and co-workers^[85] have reported the longest stability reached from MAPbBr₃ PNCs in extreme polar conditions around 600 days (1.5 years) (stability was observed by estimating the PLQY under UV excitation light), by chemically cross-linking the long-chain oleic acid and oleylamine ligands to a methacrylate-functionalized matrix. By considering that this polymeric matrix exhibits a moisture transmission rate about 4 g m⁻² day⁻¹, a low concentration of H₂O molecules can penetrate the matrix to interact with the PNCs. Water is able to passivate Br⁻ vacancies emerged in the perovskite, compensating the formed undercoordinated Pb (also known as metallic Pb) and reducing the density of nonradiative carrier traps. Thus, PNCs keep a relatively high PLQY ≈70% in aqueous solutions based on HCl, NaOH (Figure 4C), ethylene glycol, and ethanol (Figure 4D) for a long time, avoiding the material degradation. This strategy would be desirable to establish long-term stable PNCs electrodes with enhanced PL and electronic properties in real harsh scenarios.

Another alternative to passivate the PNCs surface to be stable in polar environments is through the use of some alkylammonium halide species with high binding capability such as didodecylammonium bromide (DDAB). According to the work of Ma and co-workers,^[86] DDAB acts as a capping agent, increasing the durability of CsPbBr₃ synthesized in a Pb- and Br-rich medium. Due to this capping agent effect, the formation of PbBr₂ adlayers

on the photomaterial surface is favored. Br⁻ anions would compensate halide vacancies from the PNCs, while DDA⁺ present a high affinity for Br⁻ species, that create a dense ligand package on the material surface.^[87] In this way, the branched structure of DDA⁺ induces a strong steric hindrance, which avoids to the direct interaction of polar molecules with the PNCs. Accordingly, DDAB-modified CsPbBr₃ PNCs retains the 95% of the initial PL features after 6 h in the presence of ethanol, compared to a pristine CsPbBr₃ PNCs in the absence of the capping ligand, only preserving ≈18% from their initial PL value. In the same line, Mattoussi and co-workers^[88] have mentioned the use of polysalt ligands composed by quaternary ammonium or imidazolium bromide species to provide an adequate ligand passivation to be stable in high polar alcohols such as methanol and ethanol for more than 8 months (stability was observed by measuring the PLQY under UV excitation light). The multicoordination of the PNCs to compensate surface defects and the use of the above short-alkyl chains in combination with poly (isobutylene-alt-maleic anhydride) (which can be easily dispersed in the alcoholic media) are the main reasons to prepare modified green-emitting PNCs with long-term stability in the polar environment. In general, the passivation strategy of PNCs to fabricate more stable photoelectrodes for solar-driven reactions is still at an initial stage. It is apparent that the compensation of defects in the photoactive materials via incorporation of ligands

mediates a balance between long-term stability and enhanced carrier transfer ability or supported by electrolyte solution to increase the PEC activity of the electrode.

3.3. Synthetic Protocols to Prepare Intrinsically Stable PNCs in Polar Media for Potential PEC

The above alternatives can avoid the direct interaction of the PNCs with the polar molecules, keeping intact the PL and PEC properties. But eventually, these species (specially H₂O and O₂) can permeate the protective layer, deteriorating the PNCs at a certain stage. Therefore, the synthesis of PNCs that can directly interact with polar environments would be ideal to provide long-term PEC capability for oxidation/reduction reactions.

In this context, Zhang and co-workers^[89] have obtained water-tolerant cobalt-doped CsPbBr₃/Cs₄PbBr₆ PNCs (Co@ CsPbBr₃/Cs₄PbBr₆) through ligand-assisted reprecipitation (LARP), using hexafluorobutyl methacrylate (HFBMA) as a ligand stabilizer, to study the PEC behavior of the material for CO₂ reduction directly in H₂O medium. While HFBMA ligand shows a higher binding capability to the PNCs surface through F atoms, the presence of 2% Co²⁺ promotes an efficient carrier separation/transfer from host nanocrystals to Co cocatalyst. This behavior was first

evidenced by linear sweep voltammetry measurements, where electrons from PNCs can be transferred via CB (−1.09 V versus NHE) to the surface energy levels provided by Co²⁺ doping (−0.76 V versus NHE). Thus, Co²⁺ sites show a high enough reducing power to favor the CO₂ transformation mainly into CO. Thus, an increase in the photocurrent was obtained for the Co@ CsPbBr₃/Cs₄PbBr₆ material in the presence of Co²⁺ (≈doubling the photoresponse of the pristine CsPbBr₃/Cs₄PbBr₆) (Figure 5A) in a 0.1 M KCl aqueous solution, validating the enhanced charge carrier separation and transport to mediate the CO₂ reduction. Accordingly, the Co-doped PNCs exhibit a performance for PC CO₂ reduction ≈239 μmol g^{−1} for CO, which is five times higher compared to that obtained for pristine photomaterial (Figure 5B). This material is stable during this reaction around 20 h. However, its stability in PEC systems has not been reported.

The long-term stability of the Co@CsPbBr₃/Cs₄PbBr₆ composite is associated to the hydrolysis of HFBMA to produce its amphiphilic form known as hexafluorobutanol. This species exhibits a C—OH head in the presence of H₂O, making that the PNCs composite is soluble in this solvent and shows a high green-emission at the same time. Accordingly, the integration of the PNCs with a cocatalyst

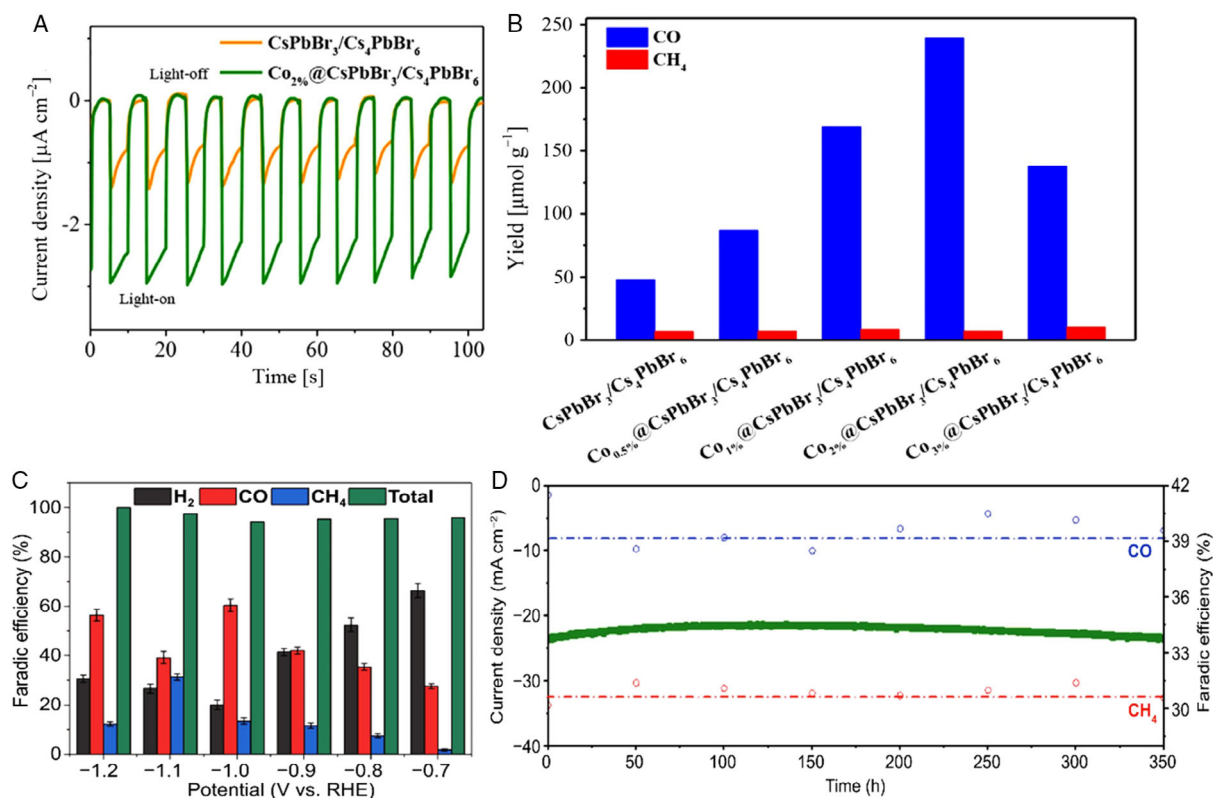


Figure 5. A) Photocurrent transient measurements of undoped CsPbBr₃/Cs₄PbBr₆ and Co_{2%}@CsPbBr₃/Cs₄PbBr₆ electrodes (at −0.4 V versus Ag/AgCl) and B) performance of the PC CO₂ reduction to produce CH₄ through Co-doped CsPbBr₃/Cs₄PbBr₆ photocatalyst by varying the concentration of Co²⁺ doping (0.1 M KCl aqueous solution, simulated solar light, AM1.5G). Reproduced with permission.^[89] Copyright 2019, John Wiley & Sons, Inc. C) Faradaic efficiencies in function of the applied potential (vs RHE) during the electrocatalytic CO₂ reduction to produce H₂, CO, CH₄ and D) long-term stability measurement by using w-CsPbBr₃ PNCs electrodes (0.1 M KHCO₃ aqueous solution). Reproduced under the terms of the CC-BY license.^[92] Copyright 2021, The Authors. Published by Springer Nature.

in an aqueous solution is an interesting option to mediate the CO₂ reduction. However, this strategy will be impactful if the metal doping could be extended to a wide range of metals with high capacity to perform reduction reactions, for instance, Pt, Cu, and Al, among others.

On the other hand, Fan and co-workers^[90] have reported a novel short-chain ligand-based hot-injection synthetic protocol for the preparation of CsPbBr₃ PNCs powders with highly oxidizing power to perform the degradation of tetracycline hydrochloride antibiotic (TC-HCl) in ethanol and water. By analyzing the PEC response of the material evaluated as a photoelectrode in aqueous conditions through photocurrent transient measurements, it is clear that a low photocurrent in the nanoscale range is obtained, indicating the degradation of the nanocrystals. However, this photocurrent is almost stable for 4 h after seven light on/off cycles. In addition, a performance ≈18% was achieved in the TC-HCl degradation in this polar medium, indicative that the perovskite still drives oxidation reactions. The authors associated this feature to the formation of CsPb₂Br₅ crystal structure considering that CsBr from the nanocrystals can be easily dissolved in water. Although the authors did not study in detail the influence of CsPb₂Br₅ perovskite, the results point out that this species is involved in the PEC behavior of the nanocrystals in water. According to the literature, CsPb₂Br₅ can act as a protective layer assembled to CsPbBr₃, also transferring carriers to the 3D material and improve its PL properties.^[91] Thus, it is inferred that the PC activity of CsPbBr₃ can be boosted by the presence of the 2D material. Then, by changing the polar solvent to ethanol, the performance of TC-HCl degradation increased up to 76% and no presence of CsPb₂Br₅ was observed. A solvent with a lower polarity makes that the photocatalyst is not rapidly deteriorated, being available to trigger the solar-driven oxidation reaction.

Meantime, Prasad and co-workers^[92] have established a modification in the hot-injection synthesis of CsPbBr₃ PNCs, by promoting their growth in a Cs⁺/Br⁻ rich mixture reaction. These nanocrystals are stable in water for 200 days (w-CsPbBr₃), which is desirable for leading the efficient electrocatalytic (EC) CO₂ reduction. No illumination was required to perform the EC reduction reaction. Compared to the conventional synthetic protocol, where the PNCs are commonly prepared in a Pb-rich environment, the excess of Cs⁺ and Br⁻ species generate the mixture based on CsBr/Cs₄PbBr₆, which show no optical properties. After H₂O addition, CsBr is dissolved, whereas Cs₄PbBr₆ is transformed to 3D CsPbBr₃ by leaching Cs⁺ and Br⁻ species. Then, while CsPbBr₃ is losing surface ligands in the presence of the polar solvent, the dissolved CsBr can fill the ligand and halide vacancies, inducing a suitable surface passivation to provide long-term stability to the nanocrystals. Therefore, CsPbBr₃ PNC electrodes were fabricated to trigger the CO₂ reduction in 0.1 M KHCO₃ aqueous solution, generating mainly H₂, CO, and CH₄ with maximum Faradaic efficiencies ≈70% (at -0.7 V versus NHE), 40% and 32% (at -1.1 V versus NHE), respectively (Figure 5C). This material is also long-term stable, performing the EC CO₂ reduction for 350 h (Figure 5D). Cubic morphology of PNCs is preserved after reaction, corroborating this stability.

4. PEC Behavior of Lead-Free PNCs

Although Pb-PNCs are considered the most promising photocatalysts to improve the performance in PEC systems, it is also true that these materials present the inherent Pb toxicity, hindering their large-scale implementation. Thus, research groups are interested in studying the synthesis of lead-free perovskites, where some structures such as Cs₂AgBiBr₆,^[93–96] Cs₃Sb₂X₉ (X = Br, I),^[97–99] DMASnBr₃,^[100] and Cs₃Bi_{2x}Sb_{2–2x}I₉^[101] have been applied for PC H₂ production and CO reduction reactions. However, these materials show a high density of structural defects, wide bandgap. Additionally, some nontoxic elements such as Sn, Sb can be easily oxidized. These disadvantages make difficult the preparation of a suitable photoelectrode. Therefore, the state-of-the-art strategies to stabilize Pb-free PNCs in polar solvents are scarce. Nevertheless, there is a couple of contributions where the PEC behavior of these attractive photomaterials in polar media is reported.

Kuang and co-workers^[102] have synthesized Cs₂SnI₆ PNCs/SnS₂ nanosheets hybrid composites by carrying out the combination of different amount of CsI precursor solution and SnS₂ nanosheets through stirring. The deposition of Cs₂SnI₆ nanocrystals on the SnS₂ expands the light-harvesting efficiency of the composite material in the wavelength range 600 to 900 nm, indicating an improvement of carrier photogeneration. This enhancement was verified through photocurrent transient measurements, where the highest photocurrent ≈35 μA cm⁻² was obtained for the hybrid composite prepared from 2 mM CsI (Cs₂SnI₆(1.0)/SnS₂) (Figure 6A). By using transient absorption spectroscopy measurements, authors conclude that the PNCs can inject electrons to the sheets, while this later transfer holes to the perovskite (II-type heterostructure). In this way, carrier recombination is avoided (Figure 6B). Although these measurements were conducted in ammonium hexafluorophosphate (APF₆)/dichloromethane, the trend between the different composites supports their ability to perform the CO₂ reduction in a polar media containing H₂O and methanol. Accordingly, Cs₂SnI₆(1.0)/SnS₂ shows the highest CO₂ conversion to CH₄ with a performance ≈6.09 μmol g⁻¹. This value is not declined after three cycles of reaction for 3 h, indicating the high stability of the material (Figure 6C).

One alternative to maximize the PC and PEC activity of Cs₂SnI₆ PNCs based photocatalysts is through the use HI aqueous solutions and the deposition of cocatalysts, where this type of perovskite has exhibited a high stability. Guo and co-workers^[103] have studied the improvement of hydrogen production by using Pt–I₃ sites Cs₂SnI₆ (PtSA/Cs₂SnI₆) powders in this polar media. They concluded that the efficient carrier transfer is promoted from the perovskite to the metal, which is coordinating with three iodide species from the perovskite surface. This enhanced charge separation was evidenced through photocurrent transient measurements (Figure 6D) in 0.1 M TBAPF₆/dichloromethane, being the highest photocurrent (≈10 mA cm⁻²) obtained for the PtSA/Cs₂SnI₆ heterostructure, compared to the Cs₂SnI₆ and Pt-nanoparticle/Cs₂SnI₆ (PtNP/Cs₂SnI₆) reference systems. Therefore, H₂ production was triggered in a HI aqueous solution containing 20 vol% H₃PO₂, with a performance closer to 3000 μmol g⁻¹, being its reducing power stable for 180 h (Figure 6E).

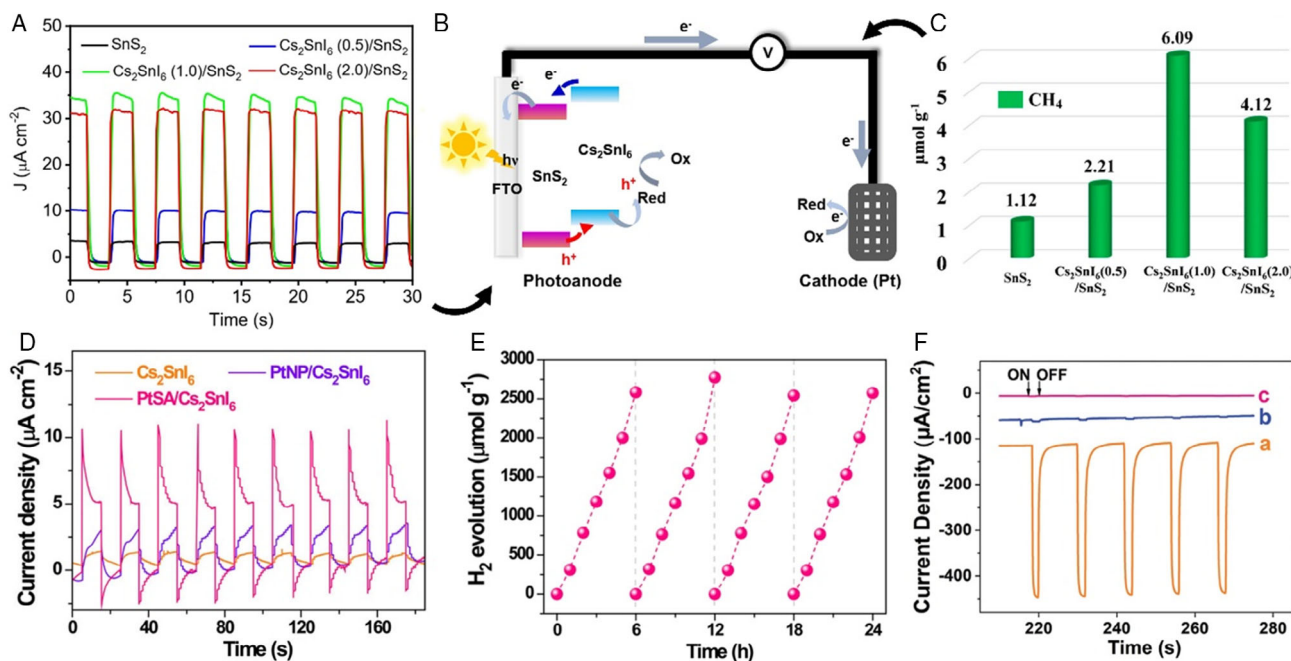


Figure 6. A) PEC behavior of Cs₂SnI₆(X)/SnS₂ (X = 0.5, 1.0, 2.0) heterostructure-based photoelectrodes in a 0.1 M APF₆/dichloromethane electrolyte solution. B) Schematic representation of charge separation and transport into II-type Cs₂SnI₆(X)/SnS₂ composite material into a PEC cell. C) PC activity for CO₂ transformation to CH₄ by using Cs₂SnI₆(X)/SnS₂ (X = 0.5, 1.0, 2.0) in a H₂O/methanol media. Reproduced with permission.^[102] Copyright 2019, American Chemical Society. D) PEC behavior of Cs₂SnI₆, PtNP/Cs₂SnI₆ and PtSA/Cs₂SnI₆ based photoelectrode in a 0.1 M TBAPF₆/dichloromethane solution (at 0 V versus Ag/AgCl). E) Cyclic stability measurements for PtSA/Cs₂SnI₆ photocatalyst during H₂ production in a HI aqueous solution containing 20 vol% H₃PO₂ (visible illumination, UV-cut-off filter). Reproduced under the terms of the CC-BY license.^[103] Copyright 2021, The Authors. Published by Springer Nature. F) PEC behavior Cs₂PtBr₆/GCE (orange line); Cs₂PdBr₆/GCE (blue line) and CsPbBr₃/GCE electrodes (magenta line) conducted in a 0.1 M PB solution, pH 7.4 (at -0.6 V versus Ag/AgCl, UV illumination). Reproduced with permission.^[104] Copyright 2021, John Wiley & Sons, Inc.

Then, Peng and co-workers^[104] have introduced the synthesis of Cs₂PtBr₆ PNCs deposited on glassy carbon electrodes (GCE), in order to observe their stability and PEC capability in phosphate aqueous media. By depicting an ordered-vacancy structure and a bandgap around 1.32 eV (covering all the visible region), the photoelectrode produces a higher cathodic photocurrent density $\approx 335 \mu\text{A cm}^{-2}$ in 0.1 M PB solution, pH 7.4, which is much higher compared to CsPbBr₃ and Cs₂PdBr₆ reference systems (Figure 6F). Furthermore, a repeatable photoresponse was obtained after 30 light on/off cycles indicating the long-term stability of the PNCs. This photocurrent showed a slight decrease after 60 days at relative humidity of 55%, indicating their ultralong-term stability. Interestingly, the photomaterial exhibits photocurrent at excitation wavelength of 940 nm, opening the door to perform future contributions of solar-driven applications under UV-vis-IR irradiation conditions.

Lastly, we propose that some Sn-based emitting perovskite nano- and microcrystals can also be interesting to be explored as PC and PEC systems. This is the case of organic A₂SnBr₆ (A = OCTAm⁺; octylammonium, OLAm⁺; oleylammonium).^[105,106] These materials show a PLQY higher than 80%, being luminescent in the orange region. However, by performing halide composition engineering as the case of their Pb-analogous, bandgap and relative positions would be

modulated to lead oxidation/reduction reactions in low and high polar media, being more attractive the latter condition. In this case, OCTA₂mSnBr₆ 2D perovskites are synthesized from aqueous solutions, which confers them an inherent stability in this medium.^[105] Therefore, these materials are found suitable to perform the main solar-driven reactions discussed above.

We note that thus far the performance of the perovskite-based photocatalysts to conduct solar-driven reactions as CO₂ reduction seems to be increasing; part of the state-of-the-art does not consider the influence of the photolysis/photocatalytic oxidation of the environment (solvent where the reactions take place), on the generation of the expected products. This is the case of alcohols such as MeOH, which is used as a hole scavenger to avoid the carrier recombination into the photocatalyst, and thereby, reduction reactions can be efficiently led. However, the MeOH photooxidation produces CO₂ and H₂, which can interfere in the estimation of the real photocatalytic performance and the product selectivity. Therefore, it is crucial to carry out control experiments in the absence of the photomaterial in these solvents to validate the nature of products formed by the oxidation/reduction of the environment. Labeling experiments are also needed to confirm the chemical origin of the obtained products.

Table 1. Photo(electro)catalytic performance analysis of the reported state-of-the-art PNCs in low/high polar environments. Parameters such as electrolyte/type of environment, solar-driven reaction, stability, and result of performance have been considered for the PNCs in function of their oxidizing/reducing nature.

Solar-driven reactions in nonpolar environments					
Photomaterial	Electrolyte (under AM1.5G light)/ nonpolar/polar environment	Solar- driven reaction	Stability	Performance indicator	References
CsPbBr ₃ -GO PNCs	CO ₂ -saturated ethyl acetate/H ₂ O	CO ₂ reduction	>12 h	CO ₂ transformation in H ₂ (≈1.58 μmol g ⁻¹), CO (≈58.7 μmol g ⁻¹), and CH ₄ (29.6 μmol g ⁻¹)	[62]
GO-wrapped MAPbBr ₃ PNCs	CO ₂ -saturated 0.1 M TBAPF ₆ in propylene carbonate	CO ₂ reduction	≈2.2 h	CO ₂ transformation to CO (0.525 μmol g ⁻¹) and CH ₄ (0.025 μmol g ⁻¹)	[63]
Mixed halide CsPbBr _{3-x} I _x PNCs/ CNT	0.1 M TBAPF ₆ + 4 mM benzoquinone in dichloromethane	Organic oxidation	–	Improvement of photocurrent 7.7-fold over the pristine CsPbBr ₃	[64]
CsPbBr ₃ PNCs	0.03 mM 2-MBT in hexane (visible light)	Organic oxidation	–	Total degradation of 2-MBT after 120 min	[43]
CsPbBr ₃ PNCs	0.1 M TBAPF ₆ + 0.05 M BzOH/0.05 M BzCHO in dichloromethane	Oxidation/reduction reaction	–	BzOH oxidation ≈12%, operation of a tandem photoanode/photocathode fuel cell	[66]
Encapsulation of PNCs—formation of heterostructures					
CsPbBr ₃ @Ni ₂ P	0.01 M phosphate buffer aqueous solution at pH 7.4	HER	12 h	Benchmark photocurrent of 900 μA cm ⁻² , enhancement of HER process 10 000-fold than pristine CsPbBr ₃	[71]
CsPbBr ₃ PNCs/m-SiO ₂	Water, aqua regia, saline water	–	1 month	Preserve the PL properties of PNCs, PLQY ≈89%	[75]
CsPbBr ₃ PNCs @PCN-333(Fe)	1 M LiTFSI/TEGDME	ORR, OER	> 1 h	O ₂ evolution/consumption: 1.77 μmol of O ₂ in the ORR and 1.74 μmol of O ₂ for reversed OER.	[80]
TiO ₂ (N-C)/CPB/TiO ₂	0.1 M Na ₂ SO ₄ /glycerol aqueous solution, pH 2	Organic oxidation	> 0.5 h	Transformation of glycerol into glyceraldehyde (≈450 mmol m ⁻² h ⁻¹) and 1,3-dihydroxyacetone (140 mmol m ⁻² h ⁻¹)	[81]
Surface passivation engineering					
MAPbI ₃ single crystals	0.36 M MABr, acetonitrile/methanol solution	Photoelectrosynthesis	6 h	Faradaic efficiency ≈93% for the DMDF production	[83]
Methacrylate-modified MAPbBr ₃ PNCs	HCl, NaOH, ethylene glycol and ethanol aqueous solutions	–	600 days (1.5 years)	Preserving the PLQY ≈70% in harsh conditions	[85]
DDAB-modified CsPbBr ₃ PNCs	Ethanol	–	6 h	Preserving the PL feature ≈95% from initial value	[86]
Polysalt ligands in CsPbBr ₃ PNCs	Methanol/ethanol	–	8 months	High PLQY ≥ 95% in the polar media	[88]
Synthetic protocols to prepare intrinsically stable PNCs in polar media for potential PEC					
Co@ CsPbBr ₃ /Cs ₄ PbBr ₆ PNCs	0.1 M KCl aqueous solution	CO ₂ reduction	20 h	CO ₂ transformation to CO (239 μmol g ⁻¹), 5-fold higher than pristine photomaterial	[89]
CsPbBr ₃ PNCs	Water and ethanol aqueous solution + 10 mg L ⁻¹ TC-HCl	Organic oxidation	–	Degradation of TC-HCl antibiotic ≈18% in a polar solvent	[90]
Cs ⁺ /Br ⁻ -enriched CsPbBr ₃ PNCs	0.1 M KHCO ₃ aqueous solution	CO ₂ reduction	350 h	CO ₂ transformation to H ₂ , CO and CH ₄ , with Faradaic efficiencies ≈70%, 40%, and 32%, respectively.	[92]
PEC behavior of lead-free PNCs					
Cs ₂ SnI ₆ PNCs/SnS ₂ nanosheets	CO ₂ -saturated methanol aqueous solution, (150 mW cm ⁻² , 400 nm filter)	CO ₂ reduction	3 h (three cycles of reaction)	CO ₂ conversion to CH ₄ (performance ≈6.09 μmol g ⁻¹)	[102]

Table 1. Continued.

Solar-driven reactions in nonpolar environments					
Pt-I ₃ sites Cs ₂ SnI ₆	HI aqueous solution containing 20 vol% H ₃ PO ₃ , visible illumination	H ₂ production	180 h	H ₂ generation with a performance ≈3000 μmol g ⁻¹	[103]
Cs ₂ PtBr ₆ PNCs/GCE	0.1 M phosphate buffer aqueous solution at pH 7.4	Study of PEC properties	60 days	Constant photocurrent density ≈335 μA cm ⁻² at 55% relative humidity	[104]

Lastly, we summarize the PEC applications performed by PNCs highlighted in each section, to evidence the most relevant results obtained according to their oxidizing/reducing nature.

As shown in **Table 1**, most of the applications are focused on the CO₂ reduction to added-value products such as CO, CH₄, and H₂, with high performances and the oxidation of organic compounds. Clearly, the encapsulation of PNC or the development of heterostructures shows a clear advantage over existing alternatives to protect PNCs from polar environments, deducing that the incorporation of inorganic layers improves the carrier separation and transport from the PNCs, accumulating more electrons/holes and thereby increase the reducing/oxidizing power of the photocatalyst. On the other hand, the surface passivation engineering is an unexplored alternative to prepare efficient photomaterials and conduct PEC reactions. As modified

PNCs can reach up to 600 days of stability in harsh media, a balance between a suitable concentration of capping ligands and the ability of charge transfer will be ideal to fabricate competitive photocatalyst with improved photo(electro)catalytic properties.

5. Charge Transfer Kinetics in PNCs

After highlighting the recent and promising strategies to make more stable PNCs and conduct PEC reactions in polar solvents, it is also relevant to address the charge carrier dynamics in PNCs, and the direct interaction with donor and acceptor agents. In this field, the interfacial charge transfer between PNCs and redox probes/organic molecules proceeds has been widely studied,

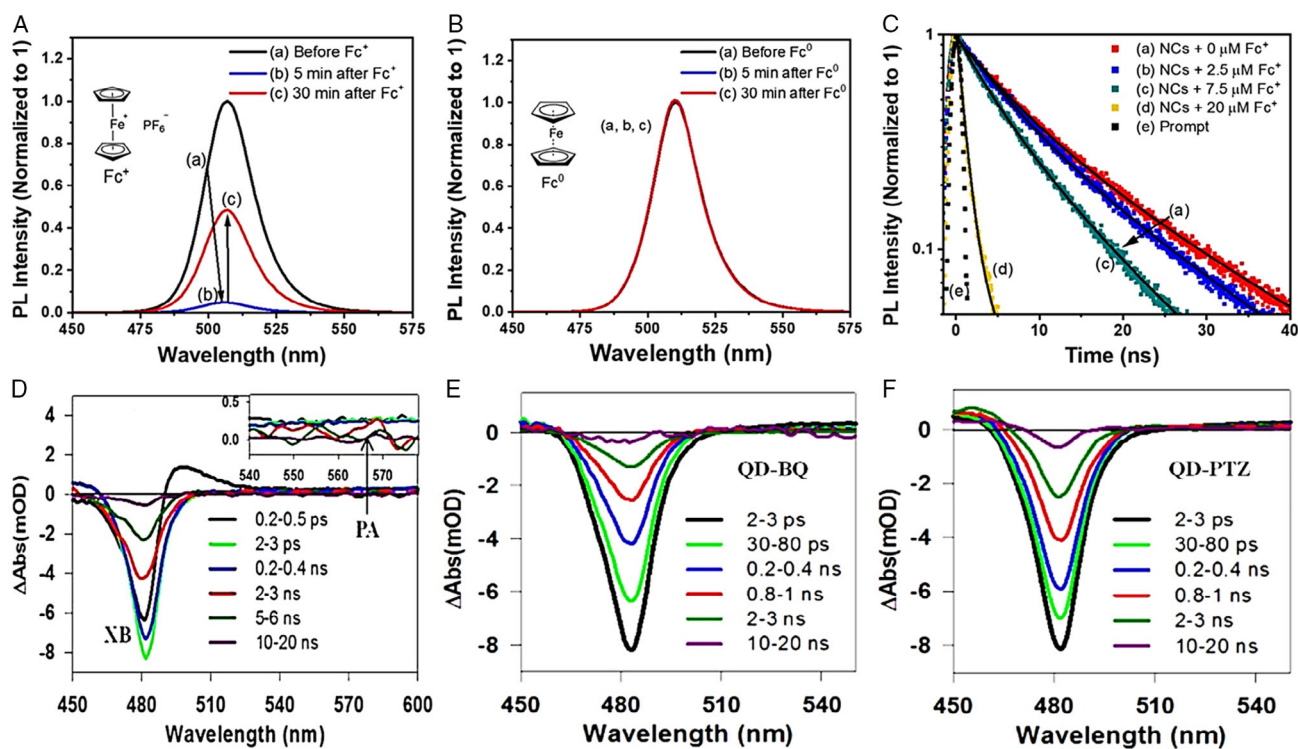


Figure 7. PL spectra of CsPbBr₃ PNCs acquired at 430 nm, after the addition of A) 7.5 μM Fc⁺ and B) 7.5 μM Fc⁰: (a) in absence of Fc⁺ (Fc⁰), (b) after 5 min, and (c) 30 min of the Fc⁺ (Fc⁰) addition. C) Time-resolved PL decay of CsPbBr₃ tracked at 509 nm, by varying the Fc⁺ concentration: (a) 0, (b) 2.5, (c) 7.5, and (d) 20 μM. (e) Instrument response. Reproduced with permission.^[107] Copyright 2019, American Chemical Society. TA spectra for CsPbBr₃, D) in the absence of organics, and the presence of E) BQ and F) PTZ molecules, at indicated time delays (400 nm excitation). Reproduced with permission.^[108] Copyright 2015, American Chemical Society

as well as the formation of heterostructures to resist polar solvents, and their impact on the promotion of excited state interactions, and thereby the efficiency of the photocatalytic activity.

In a first approach, Kamat and co-workers^[107] have studied how the CsPbBr₃ PNCs can be photocatalytically active in the presence of a redox mediator such as ferrocenium/ferrocene (Fc⁺/Fc⁰), deducing the carrier transfer mechanism involved into the process. By using optical spectroscopic tools such as steady state (Figure 7A,B) and time-resolved PL measurements (Figure 7C), different dynamics of the quenching of the radiative recombination at low and high concentrations of Fc⁺ were observed. Here, the optical properties of Fc⁰ kept intact, indicating that carrier transfer is not occurring between PNCs and the reduced form of Fc⁺ (no oxidation induced by PNCs). Thus, at low Fc⁺ concentrations, this species is quickly consumed during the reduction step in the PNCs/solution interface, allowing CsPbBr₃ PNCs to recover their emission feature after some minutes. However, at higher Fc⁺ concentrations, the PNCs surface is still rich in Fc⁺. When this species is reduced to Fc⁰, it moves away from the photocatalyst/solution interface, allowing new Fc⁺ to interact with the PNCs. Only after 16 h of continuous reaction, PL recovery was reached. The decrease of the PL lifetime of the PNCs by increasing the Fc⁺ concentration allowed to corroborate this finding, as the recombination was decreased by electron transfer to a higher density of Fc⁺. Therefore, PNCs show photocatalytic activity to reduce Fc⁺ and recover their optical properties at low electron acceptor concentrations.

On the other hand, Lian and co-workers^[108] have reported an alternative way to observe the interfacial carrier transfer dynamics into CsPbBr₃ PNCs through ultrafast transient absorption spectroscopy. PNCs show a high PLQY ≈79%, which is attributed to the electron- and hole-trapping processes, also deducing that the decay of the lowest excitonic states follows a monoexponential behavior with a lifetime ≈4.5 ± 0.2 ns. With the purpose to evidence the electron and hole transfer capability of PNCs, the authors have introduced benzoquinone (BQ, electron acceptor) and phenothiazine (PTZ, hole acceptor) and observe the carrier dissociation. Compared to the corresponding recombination dynamics of CsPbBr₃ in the absence of organics (Figure 7D), electron and hole transfer from CsPbBr₃ to BQ (Figure 7E) and PTZ (Figure 7F) were faster, with half-lives ≈65 ± 5 and 49 ± 6 ps, respectively. The authors concluded that in the presence of species to conduct solar-driven reactions, the recombination rate into PNCs is slower compared to the carrier transfer or injection to produce oxidized/reduced species.

Lastly, regarding the applications of PNCs in polar environments, which was the main topic of this review, Kamat and co-workers^[109] have studied the effect of the deposition of CdS nanoparticles decorating CsPbBr₃ PNCs, to increase their stability in polar solvents. The authors claim that optical properties and stability of the nanocrystals are associated to the passivation of surface defects, which also act as a coverage avoiding the direct interaction with polar species. To observe how the formation of a heterostructure influences the interfacial carrier transfer, femtosecond transient absorption spectroscopy was conducted in the presence of ethyl viologen (a probe electron acceptor). It was deduced that the average electron transfer rate estimated to be ≈6.5 × 10¹⁰ s⁻¹ was lower compared to that of conventional oleic acid/oleylamine capped PNCs

(≈3.6 × 10¹¹ s⁻¹). This discrepancy is associated to the decrease of surface interactions between the photocatalyst and the viologen, by the presence of CdS layer (mainly lack of interactions between organic ligands and the viologen). Nevertheless, the heterostructure can accumulate more electrons coming from the PNCs to more efficiently carry out the viologen reduction, compared to the pristine CsPbBr₃. Therefore, the surface properties of modified PNCs to resist highly polar environments can also impact on the carrier transfer, affecting the photocatalytic power of the photomaterial.

6. Conclusions and Outlooks

In this review, we have discussed the main alternatives proposed in the current state of the art to improve the stabilization of PNCs in polar solvents, keeping their intrinsic properties and providing potential PEC activity for solar-driven reactions. Even though the low-polar media ensure the structural integrity of PNCs, their PEC operation can be maximized in polar environments. For this goal, strategies as encapsulation by inorganic protective layers to produce diverse heterostructures boost the PEC performance of PNCs in OER, ORR, HER CO₂ reduction reactions, and organics degradation, hindering the permeation of polar molecules to deteriorate the nanocrystals. The deposition of thin metal/metal oxide layers and the addition of capping ligands to fill/replace surface defects are an interesting surface passivation alternative to improve the photophysical features and carrier generation into the PNCs, making them highly stable in harsh conditions such as strong acids, bases, high polar targeted molecules, etc. Both the abovementioned approaches are complementary to the synthesis of PNCs with intrinsic resistance to polar solvents, mediating a closer interaction between the photocatalyst and the polar molecules, to enhance the PEC ability and provide long-term stability to the photomaterial.

From our point of view and based on the current literature, studies about the influence of surface passivation engineering on the PEC behavior of PNCs are still an unexplored topic. This is deduced from the scarce reports concerning the preparation of PNCs photocatalyst for PEC applications even when the stability issues of the photomaterials are overcome. Attending to our experience in the PNCs synthesis and fabrication of thin films for PEC systems, the presence of a high density of ligands based on hydrocarbon chains produces an insulating layer for the deposited material, restraining the carrier extraction and transport. Therefore, a compromise between the density of cappings to keep the material stability and simultaneously reach a high charge transport/transfer kinetics should be focused. This balance can offer a gamut of opportunities to develop more stable and efficient organic-inorganic PNCs photoelectrodes, including those that can be fabricated from less-defective lead-free PNCs.

In this way, by avoiding the oxidation of the metal replacing Pb positions into the photomaterial would guarantee the fabrication of “more ecofriendly” photocatalysts with promising oxidizing/reducing activity in PEC processes. On the other hand, it is also relevant to highlight that the reaction environment can also participate in the generation/selectivity of new products from photo(electro)catalytic reactions, and their contribution cannot be ignored. Consequently, the use of well-designed control

experiments is mandatory to validate the photocatalytic and photoelectrochemical performance of PNCs. Lastly, obtaining valuable information about the carrier transfer dynamics of PNCs is essential to understand how the electron/hole acceptor is interacting with the photocatalyst and explain their oxidizing/reducing behavior. In general, the field of photo- and photo (electro)catalysis led by PNCs are still at their infancy, and the purpose of this contribution is to provide key approaches to advance in the development of photoelectrodes with high photoredox activity for the most impactful solar-driven systems.

Acknowledgements

The authors acknowledge financial support by European Research Council (ERC) via Consolidator Grant (724424-No-LIMIT) Ministry of Science, Innovation of Spain under Projects STABLE (PID2019-107314RB-I00), ELECTROVAL (PID2020-116093RB-C41), Generalitat Valenciana via Prometeo Grants (Prometeo/2018/098 and PROMETEO/2020/028), APOSTD grant (APOSTD/2021/251), Universitat Jaume I, through UJI project (UJI-B2020-50) and postdoctoral grant POSDOC/2019/20.

Conflict of Interest

The authors declare no conflict of interest.

Keywords

perovskite nanocrystals, photo(electro)catalysis, polar solvents, solar-driven reactions, stability

Received: January 6, 2022

Revised: March 2, 2022

Published online:

- [1] H. Huang, B. Pradhan, J. Hofkens, M. B. J. Roeffaers, J. A. Steele, *ACS Energy Lett.* **2020**, *5*, 1107.
- [2] G. Gao, Q. Xi, H. Zhou, Y. Zhao, C. Wu, L. Wang, P. Guo, J. Xu, *Nanoscale* **2017**, *9*, 12032.
- [3] B. O. Oromolade, O. A. Arotiba, *Sci. Rep.* **2020**, *10*, 5348.
- [4] M. Bellardita, V. Loddo, F. Parrino, L. Palmisano, *ChemPhotoChem* **2021**, *5*, 767.
- [5] N. S. Lewis, D. G. Nocera, *Proc. Natl. Acad. Sci.* **2006**, *103*, 15729.
- [6] S. Berardi, S. Drouet, L. Francàs, C. Gimbert-Suriñach, M. Guttentag, C. Richmond, T. Stoll, A. Llobet, *Chem. Soc. Rev.* **2014**, *43*, 7501.
- [7] K. Villa, J. R. Galán-Mascarós, N. López, E. Palomares, *Sustainable Energy Fuels* **2021**, *5*, 4560.
- [8] Y. Wang, D. He, H. Chen, D. Wang, *J. Photochem. Photobiol., C* **2019**, *40*, 117.
- [9] K. Maeda, *J. Photochem. Photobiol., C* **2011**, *12*, 237.
- [10] F. J. Mancilla, S. F. Rojas, A. F. Gualdrón-Reyes, M. I. Carreño-Lizcano, L. J. Duarte, M. E. Niño-Gómez, *RSC Adv.* **2016**, *6*, 46668.
- [11] T. Takata, J. Jiang, Y. Sakata, M. Nakabayashi, N. Shibata, V. Nandal, K. Seki, T. Hisatomi, K. Domen, *Nature* **2020**, *581*, 411.
- [12] M. Grätzel, *Nature* **2001**, *414*, 338.
- [13] J. Zhang, J. Cui, S. Eslava, *Adv. Mater.* **2021**, *11*, 20031111.
- [14] R. Zhang, Q. Wang, J. Zhang, Q. Lu, W. Liu, S. Yin, W. Cao, *Nanotechnology* **2019**, *30*, 434001.
- [15] M. Antoniadou, V. M. Daskalaki, N. Balis, D. I. Kondarides, C. Kordulis, P. Lianos, *Appl. Catal., B* **2011**, *107*, 188.
- [16] R. Fernández-Climent, S. Giménez, M. García-Tecedor, *Sustainable Energy Fuels* **2020**, *4*, 5916.
- [17] J. Li, H. Chen, C. A. Triana, G. R. Patzke, *Angew. Chem., Int. Ed.* **2021**, *60*, 18380.
- [18] C. A. Mesa, L. Francàs, K. R. Yang, P. Garrido-Barros, E. Pastor, Y. Ma, A. Kafizas, T. E. Rosser, M. T. Mayer, E. Reisner, M. Grätzel, V. S. Batista, J. R. Durrant, *Nat. Chem.* **2019**, *12*, 82.
- [19] J. J. Velázquez, R. Fernández-González, L. Díaz, E. Pulido Melián, V. D. Rodríguez, P. Núñez, *J. Alloys Compd.* **2017**, *721*, 405.
- [20] T. W. Kim, K.-S. Choi, *Science* **2014**, *343*, 990.
- [21] B. Klahr, S. Gimenez, O. Zandi, F. Fabregat-Santiago, T. Hamann, *ACS Appl. Mater. Interfaces* **2015**, *7*, 7653.
- [22] C. A. Mesa, A. Kafizas, L. Francàs, S. R. Pendlebury, E. Pastor, Y. Ma, F. Le Formal, M. T. Mayer, M. Grätzel, J. R. Durrant, *J. Am. Chem. Soc.* **2017**, *139*, 11537.
- [23] T. Li, T. Kasahara, J. He, K. E. Dettelbach, G. M. Sammis, C. P. Berlinguette, *Nat. Commun.* **2017**, *8*, 390.
- [24] L. Zhang, L. Liardet, J. Luo, D. Ren, M. Grätzel, X. Hu, *Nat. Catal.* **2019**, *2*, 366.
- [25] N. Perini, C. Hessel, J. L. Bott-Neto, C. T. G. V. M. T. Pires, P. S. Fernandez, E. Sitta, *J. Solid State Electrochem.* **2021**, *25*, 1101.
- [26] A. Dey, J. Ye, A. De, E. Debroye, S. K. Ha, E. Bladt, A. S. Kshirsagar, Z. Wang, J. Yin, Y. Wang, L. N. Quan, F. Yan, M. Gao, X. Li, J. Shamsi, T. Debnath, M. Cao, M. A. Scheel, S. Kumar, J. A. Steele, M. Gerhard, L. Chouhan, K. Xu, X.-G. Wu, Y. Li, Y. Zhang, A. Dutta, C. Han, I. Vincon, A. L. Rogach, et al., *ACS Nano* **2021**, *15*, 10775.
- [27] J. Chen, C. Dong, H. Idriss, O. F. Mohammed, O. M. Bakr, *Adv. Mater.* **2019**, *10*, 1902433.
- [28] L. Protesescu, S. Yakunin, M. I. Bodnarchuk, F. Krieg, R. Caputo, C. H. Hendon, R. X. Yang, A. Walsh, M. V. Kovalenko, *Nano Lett.* **2015**, *15*, 3692.
- [29] A. F. Gualdrón-Reyes, S. Masi, I. Mora-Seró, *Trends Chem.* **2021**, *3*, 499.
- [30] F. Krieg, S. T. Ochsenbein, S. Yakunin, S. ten Brinck, P. Aellen, A. Süess, B. Clerc, D. Guggisberg, O. Nazarenko, Y. Shynkarenko, S. Kumar, C.-J. Shih, I. Infante, M. V. Kovalenko, *ACS Energy Lett.* **2018**, *3*, 641.
- [31] G. R. Yettapu, D. Talukdar, S. Sarkar, A. Swarnkar, A. Nag, P. Ghosh, P. Mandal, *Nano Lett.* **2016**, *16*, 4838.
- [32] R. Grisorio, E. Fanizza, I. Allegretta, D. Altamura, M. Striccoli, R. Terzano, C. Giannini, V. Vergaro, G. Ciccarella, N. Margiotta, G. P. Suranna, *Nanoscale* **2020**, *12*, 623.
- [33] G. Nedelcu, L. Protesescu, S. Yakunin, M. I. Bodnarchuk, M. J. Grotevent, M. V. Kovalenko, *Nano Lett.* **2015**, *15*, 5635.
- [34] M. Hao, Y. Bai, S. Zeiske, L. Ren, J. Liu, Y. Yuan, N. Zarrabi, N. Cheng, M. Chasemi, P. Chen, M. Lyu, D. He, J.-H. Yun, Y. Du, Y. Wang, S. Ding, A. Armin, P. Meredith, G. Liu, H.-M. Cheng, L. Wang, *Nat. Energy* **2020**, *5*, 79.
- [35] K. Lin, J. Xing, L. N. Quan, F. P. G. de Arquer, X. Gong, J. Lu, L. Xie, W. Zhao, D. Zhang, C. Yan, W. Li, X. Liu, Y. Lu, J. Kirman, E. H. Sargent, Q. Xiong, Z. Wei, *Nature* **2018**, *562*, 245.
- [36] Y.-H. Kim, S. Kim, A. Kakekhani, J. Park, J. Park, Y.-H. Lee, H. Xu, S. Nagane, R. B. Wexler, D.-H. Kim, S. H. Jo, L. Martínez-Sarti, P. Tan, A. Sadhanala, G.-S. Park, Y.-W. Kim, B. Hu, H. J. Bolink, S. Yoo, R. H. Friend, A. M. Rappe, T.-W. Lee, *Nat. Photonics* **2021**, *15*, 148.
- [37] D. Xing, C. C. Lin, Y. L. Ho, A. S. A. Kamal, I. T. Wang, C. C. Chen, C. Y. Wen, C. W. Chen, J. J. Delaunay, *Adv. Funct. Mater.* **2021**, *31*, 2006283.
- [38] B. Pradhan, S. Das, J. Li, F. Chowdhury, J. Cherusseri, D. Pandey, D. Dev, A. Krishnaprasad, E. Barrios, A. Towers, A. Gesquiere, L. Tetard, T. Roy, J. Thomas, *Sci. Adv.* **2020**, *6*, eaay5225.

- [39] L. Zdražil, S. Kalytchuk, M. Langer, R. Ahmad, J. Pospíšil, O. Zmeškal, M. Altomare, A. Osvet, R. Zbořil, P. Schmuki, C. J. Brabec, M. Otyepka, Š. Kment, *ACS Appl. Energy Mater.* **2021**, *4*, 6445.
- [40] R. X. Yang, L. Z. Tan, *J. Chem. Phys.* **2020**, *152*, 034702.
- [41] A. F. Gualdrón-Reyes, J. Rodríguez-Pereira, E. Amado-González, J. Rueda-P, R. Ospina, S. Masi, S. J. Yoon, J. Tirado, F. Jaramillo, S. Agouram, V. Muñoz-Sanjosed, S. Giménez, I. Mora-Seró, *ACS Appl. Mater. Interfaces* **2020**, *12*, 914.
- [42] M. Ge, Q. Li, C. Cao, J. Huang, S. Li, S. Zhang, Z. Chen, K. Zhang, S. S. Al-Deyab, Y. Lai, *Adv. Sci.* **2017**, *4*, 1600152.
- [43] D. Cardenas-Morcoso, A. F. Gualdrón-Reyes, A. B. Ferreira Vitoreti, M. García-Tecedor, S. J. Yoon, M. Solis de la Fuente, I. Mora-Seró, S. Gimenez, *J. Phys. Chem. Lett.* **2019**, *10*, 630.
- [44] S. Shyamal, N. Pradhan, *J. Phys. Chem. Lett.* **2020**, *11*, 6921.
- [45] K. Chen, X. Deng, G. Dodekatos, H. Tüysüz, *J. Am. Chem. Soc.* **2017**, *139*, 12267.
- [46] C. Lee, Y. Shin, A. Villanueva-Antolí, S. Das Adhikari, J. Rodriguez-Pereira, J. M. Macak, C. A. Mesa, S. Giménez, S. J. Yoon, A. F. Gualdrón-Reyes, I. Mora-Seró, *Chem. Mater.* **2021**, *33*, 8745.
- [47] J. A. Christians, P. A. Miranda Herrera, P. V. Kamat, *J. Am. Chem. Soc.* **2015**, *137*, 1530.
- [48] Z. Zhu, Q. Sun, Z. Zhang, J. Dai, G. Xing, S. Li, X. Huang, W. Huang, *J. Mater. Chem. C* **2018**, *6*, 10121.
- [49] J. Huang, S. Tan, P. D. Lund, H. Zhou, *Energy Environ. Sci.* **2017**, *10*, 2284.
- [50] J. Yuan, H. Liu, S. Wang, X. Li, *Nanoscale* **2021**, *13*, 10281.
- [51] H. Wang, X. Wang, R. Chen, H. Zhang, X. Wang, J. Wang, J. Zhang, L. Mu, K. Wu, F. Fan, X. Zong, C. Li, *ACS Energy Lett.* **2018**, *4*, 40.
- [52] J. Luo, H. Yang, Z. Liu, F. Li, S. Liu, J. Ma, B. Liu, *Mater. Today Chem.* **2019**, *12*, 1.
- [53] Y. Wu, P. Wang, X. Zhu, Q. Zhang, Z. Wang, Y. Liu, G. Zou, Y. Dai, M.-H. Whangbo, B. Huang, *Adv. Mater.* **2018**, *30*, 1704342.
- [54] J. Schneider, D. W. Bahnemann, *J. Phys. Chem. Lett.* **2013**, *4*, 3479.
- [55] J. Yang, B. D. Siempelkamp, D. Liu, T. L. Kelly, *ACS Nano* **2015**, *9*, 1955.
- [56] B. Murali, S. Dey, A. L. Abdelhady, W. Peng, E. Alarousu, A. R. Kirmani, N. Cho, S. P. Sarmah, M. R. Parida, M. I. Saidaminov, A. A. Zhumekenov, J. Sun, M. S. Alias, E. Yengel, B. S. Ooi, A. Amassian, O. M. Bakr, O. F. Mohammed, *ACS Energy Lett.* **2016**, *1*, 1119.
- [57] E. Mosconi, J. M. Aspiroz, F. De Angelis, *Chem. Mater.* **2015**, *27*, 4885.
- [58] S. Gonzalez-Carrero, L. Francés-Soriano, M. González-Béjar, S. Agouram, R. E. Galian, J. Pérez-Prieto, *Small* **2016**, *12*, 5245.
- [59] S. Masi, A. F. Gualdrón-Reyes, I. Mora-Seró, *ACS Energy Lett.* **2020**, *5*, 1974.
- [60] A. F. Gualdrón-Reyes, D. F. Macias-Pinilla, S. Masi, C. Echeverría-Arrodo, S. Agouram, V. Muñoz-Sanjosed, J. Rodríguez-Pereira, J. M. Macak, I. Mora-Seró, *J. Mater. Chem. C* **2021**, *9*, 1555.
- [61] L. C. Schmidt, A. Pertegás, S. González-Carrero, O. Malinkiewicz, S. Agouram, G. Mínguez Espallargas, H. J. Bolink, R. E. Galian, J. Pérez-Prieto, *J. Am. Chem. Soc.* **2014**, *136*, 850.
- [62] Y.-F. Xu, M.-Z. Yang, B.-X. Chen, X.-D. Wang, H.-Y. Chen, D.-B. Kuang, C.-Y. Su, *J. Am. Chem. Soc.* **2017**, *139*, 5660.
- [63] Q. Wang, L. Tao, X. Jiang, M. Wang, Y. Shen, *Appl. Surf. Sci.* **2019**, *465*, 607.
- [64] M.-Z. Yang, Y.-F. Xu, J.-F. Liao, X.-D. Wang, H.-Y. Chen, D.-B. Kuang, *J. Mater. Chem. A* **2019**, *7*, 5409.
- [65] S. Eigler, C. Dotzer, A. Hirsch, M. Enzelberger, P. Müller, *Chem. Mater.* **2012**, *24*, 1276.
- [66] R. Fernández-Climent, A. F. Gualdrón-Reyes, M. García-Tecedor, C. A. Mesa, D. Cárdenas-Morcoso, L. Montañes, E. M. Barea, E. Mas-Marzá, B. Julián-López, I. Mora-Seró, S. Giménez, *Sol. RRL* **2021**, 2100723.
- [67] Z.-J. Li, E. Hofman, J. Li, A. H. Davis, C.-H. Tung, L.-Z. Wu, W. Zheng, *Adv. Funct. Mater.* **2018**, *28*, 1704288.
- [68] I. Poli, U. Hintermair, M. Regue, S. Kumar, E. V. Sackville, J. Baker, T. M. Watson, S. Eslava, P. J. Cameron, *Nat. Commun.* **2019**, *10*, 2097.
- [69] C. Pornrungrroj, V. Andrei, M. Rahaman, C. Uswachoke, H. J. Joyce, D. S. Wright, E. Reisner, *Adv. Funct. Mater.* **2020**, *31*, 2008182.
- [70] V. Andrei, R. L. Z. Hoye, M. Crespo-Quesada, M. Bajada, S. Ahmad, M. De Volder, R. Friend, E. Reisner, *Adv. Mater.* **2018**, *8*, 1801403.
- [71] L. Li, L. Gan, Z. Zhang, *Adv. Mater. Interfaces* **2021**, *8*, 2100202.
- [72] Z. Zheng, L. Liu, F. Yi, J. Zhao, *J. Lumin.* **2019**, *216*, 116722.
- [73] Y. Jing, M. J. M. Merckx, J. Cai, K. Cao, W. M. M. Kessels, A. J. M. Mackus, R. Chen, *ACS Appl. Mater. Interfaces* **2020**, *12*, 53519.
- [74] Y. Liu, L. Zhang, X. Long, P. Jiang, C. Geng, S. Xu, *J. Mater. Chem. C* **2021**, *9*, 12581.
- [75] M. N. An, S. Park, R. Brescia, M. Lutfullin, L. Sinatra, O. M. Bakr, L. De Trizio, L. Manna, *ACS Energy Lett.* **2021**, *6*, 900.
- [76] M. Abdi-Jalebi, Z. Andaji-Garmaroudi, S. Cacovich, C. Stavarakas, B. Philippe, J. M. Richter, M. Alarsi, E. P. Booker, E. M. Hutter, A. J. Pearson, S. Lilliu, T. J. Savenije, H. Renssmo, G. Divitini, C. Ducati, R. H. Friend, S. D. Stranks, *Nature* **2018**, *555*, 497.
- [77] H. Tsai, S. Shrestha, R. A. Vilá, W. Huang, C. Liu, C.-H. Hou, H.-H. Huang, X. Wen, M. Li, G. Wiederrecht, Y. Cui, M. Cotlet, X. Zhang, X. Ma, W. Nie, *Nat. Photonics* **2021**, *15*, 843.
- [78] S. Wan, M. Ou, Q. Zhong, X. Wang, *Chem. Eng. J.* **2019**, *358*, 1287.
- [79] C. Zhang, W. Li, L. Li, *Angew. Chem., Int. Ed.* **2020**, *60*, 7488.
- [80] G.-Y. Qiao, D. Guan, S. Yuan, H. Rao, X. Chen, J.-A. Wang, J.-S. Qin, J.-J. Xu, J. Yu, *J. Am. Chem. Soc.* **2021**, *143*, 14253.
- [81] R. Tang, L. Wang, Z. Zhang, W. Yang, H. Xu, A. Kheradmand, Y. Jiang, R. Zheng, J. Huang, *Appl. Catal., B* **2021**, 296.
- [82] Y. Liu, Z. Wang, S. Liang, Z. Li, M. Zhang, H. Li, Z. Lin, *Nano Lett.* **2019**, *19*, 9019.
- [83] X.-D. Wang, Y.-H. Huang, J.-F. Liao, Z.-F. Wei, W.-G. Li, Y.-F. Xu, H.-Y. Chen, D.-B. Kuang, *Nat. Commun.* **2021**, *12*, 1202.
- [84] Y. Wang, Y. Ren, S. Zhang, J. Wu, J. Song, X. Li, J. Xu, C. H. Sow, H. Zeng, H. Sun, *Commun. Phys.* **2018**, *1*, 96.
- [85] J. Jang, Y. H. Kim, S. Park, D. Yoo, H. Cho, J. Jang, H. B. Jeong, H. Lee, J. M. Yuk, C. B. Park, D. Y. Jeon, Y. H. Kim, B. S. Bae, T. W. Lee, *Adv. Mater.* **2021**, *33*, 2005255.
- [86] L. J. Ruan, B. Tang, Y. Ma, *J. Phys. Chem. C* **2019**, *123*, 11959.
- [87] M. I. Bodnarchuk, S. C. Boehme, S. ten Brinck, C. Bernasconi, Y. Shynkarenko, F. Krieg, R. Widmer, B. Aeschlimann, D. Günther, M. V. Kovalenko, I. Infante, *ACS Energy Lett.* **2018**, *4*, 63.
- [88] S. Wang, L. Du, S. Donmez, Y. Xin, H. Mattoussi, *Nanoscale* **2021**, *13*, 16705.
- [89] Y. F. Mu, W. Zhang, X. X. Guo, G. X. Dong, M. Zhang, T. B. Lu, *ChemSusChem* **2019**, *12*, 4769.
- [90] X. Qian, Z. Chen, X. Yang, W. Zhao, C. Liu, T. Sun, D. Zhou, Q. Yang, G. Wei, M. Fan, *J. Cleaner Prod.* **2020**, 249.
- [91] Z.-P. Huang, B. Ma, H. Wang, N. Li, R.-T. Liu, Z.-Q. Zhang, X.-D. Zhang, J.-H. Zhao, P.-Z. Zheng, Q. Wang, H.-L. Zhang, *J. Phys. Chem. Lett.* **2020**, *11*, 6007.
- [92] K. Chen, K. Qi, T. Zhou, T. Yang, Y. Zhang, Z. Guo, C.-K. Lim, J. Zhang, I. Žutić, H. Zhang, P. N. Prasad, *Nano-Micro Lett.* **2021**, *13*.
- [93] T. Wang, D. Yue, X. Li, Y. Zhao, *Appl. Catal., B* **2020**, *268*, 118399.
- [94] Y. Wang, H. Huang, Z. Zhang, C. Wang, Y. Yang, Q. Li, D. Xu, *Appl. Catal., B* **2021**, *282*, 119570.
- [95] D. Wu, Y. Tao, Y. Huang, B. Huo, X. Zhao, J. Yang, X. Jiang, Q. Huang, F. Dong, X. Tang, *J. Catal.* **2021**, *397*, 27.
- [96] Z. He, Q. Tang, X. Liu, X. Yan, K. Li, D. Yue, *Energy Fuels* **2021**, *35*, 15005.

- [97] Q. Sun, W. Ye, J. Wei, L. Li, J. Wang, J.-H. He, J.-M. Lu, *J. Alloys Compd.* **2022**, 893, 162326.
- [98] C. Lu, D. S. Itanze, A. G. Aragon, X. Ma, H. Li, K. B. Ucer, C. Hewitt, D. L. Carroll, R. T. Williams, Y. Qiu, S. M. Geyer, *Nanoscale* **2020**, 12, 2987.
- [99] Y. Hai, W. Huang, Z. Li, D. Wu, Q. Huang, X. Tang, *ACS Appl. Energy Mater.* **2021**, 4, 5913.
- [100] L. Romani, A. Speltini, F. Ambrosio, E. Mosconi, A. Profumo, M. Marelli, S. Margadonna, A. Milella, F. Fracassi, A. Listorti, F. De Angelis, L. Malavasi, *Angew. Chem., Int. Ed.* **2020**, 60, 3611.
- [101] G. Chen, P. Wang, Y. Wu, Q. Zhang, Q. Wu, Z. Wang, Z. Zheng, Y. Liu, Y. Dai, B. Huang, *Adv. Mater.* **2020**, 32, 2001344.
- [102] X.-D. Wang, Y.-H. Huang, J.-F. Liao, Y. Jiang, L. Zhou, X.-Y. Zhang, H.-Y. Chen, D.-B. Kuang, *J. Am. Chem. Soc.* **2019**, 141, 13434.
- [103] P. Zhou, H. Chen, Y. Chao, Q. Zhang, W. Zhang, F. Lv, L. Gu, Q. Zhao, N. Wang, J. Wang, S. Guo, *Nat. Commun.* **2021**, 12, 4412.
- [104] H. Peng, L. Xu, Y. Sheng, W. Sun, Y. Yang, H. Deng, W. Chen, J. Liu, *Small* **2021**, 17, 2102149.
- [105] A. Wang, Y. Guo, Z. Zhou, X. Niu, Y. Wang, F. Muhammad, H. Li, T. Zhang, J. Wang, S. Nie, Z. Deng, *Chem. Sci.* **2019**, 10, 4573.
- [106] X. Zhang, C. Wang, Y. Zhang, X. Zhang, S. Wang, M. Lu, H. Cui, S. V. Kershaw, W. W. Yu, A. L. Rogach, *ACS Energy Lett.* **2018**, 4, 242.
- [107] J. T. DuBose, P. V. Kamat, *J. Phys. Chem. Lett.* **2019**, 10, 6074.
- [108] K. Wu, G. Liang, Q. Shang, Y. Ren, D. Kong, T. Lian, *J. Am. Chem. Soc.* **2015**, 137, 12792.
- [109] A. Kipkorir, J. DuBose, J. Cho, P. V. Kamat, *Chem. Sci.* **2021**, 12, 14815.



Andres F. Gualdrón-Reyes is a postdoc at Institute of Advanced Materials (INAM) at Universitat Jaume I (Spain). He obtained his Ph.D. in chemistry at Universidad Industrial de Santander (Colombia) in 2018. During his Ph.D. studies, he joined INAM for 6 months under the supervision of Prof. Iván Mora-Seró, focusing on the synthesis of mixed halide perovskites for light-emitting diodes free from phase segregation. Currently, he is working on the synthesis and photophysical characterization of nanocrystals (chalcogenides and perovskites), with application in photo(electro)catalysis, optoelectronics, and photovoltaics.



Camilo A. Mesa obtained his Ph.D. (2019) from Imperial College London investigating the limiting kinetic and mechanistic factors of oxidation reactions on metal oxide photoanodes for solar fuels production under the supervision of James Durrant. After the end of the Covid-19 lockdown in 2020, Camilo joined the Institute of Advanced Materials (INAM) focusing on photo- and electrocatalytic materials for solar fuels production, especially for water and organic substrates oxidation reactions in the group of Sixto Giménez. In his free time Camilo hikes and cooks better than he synthesizes materials.



Sixto Giménez received his Ph.D. in physics in 2002 from the University of Navarra. He is a full professor at Universitat Jaume I de Castelló (Spain), where he is actively involved in the development of new concepts for photovoltaic and photoelectrochemical devices based on nanoscale materials, particularly studying the optoelectronic and electrochemical responses of the devices by different microscopic and spectroscopic tools.



Iván Mora-Seró (Ph.D. physics in 2004) is a full professor at Universitat Jaume I de Castelló (Spain), leading the Group of Advanced Semiconductor (GAS) at the Institute of Advanced Materials (INAM). His research is focused on crystal growth, nanostructured devices, transport, and recombination properties, photocatalysis, characterization, and development of photovoltaic and optoelectronic devices. Recent research activities are focused on new concepts for photovoltaic conversion and light emission (LEDs and light amplifiers) based on nanoscaled devices and semiconductor materials following two main lines: semiconductor quantum dots and halide perovskites.